Supporting Information File for:

Syntheses of Deuterium-Labeled Dihydroartemisinic Acid (DHAA) Isotopologues and Mechanistic Studies Focused on Elucidating the Conversion of DHAA to Artemisinin

Kaitlyn Varela, Francis K. Yoshimoto*

Department of Chemistry, The University of Texas at San Antonio (UTSA), One UTSA Circle, San Antonio TX 78249-0698

*corresponding author: francis.yoshimoto@utsa.edu

Organic & Biomolecular Chemistry, 2024, xxxx, xxxxxx

Table of Contents

1. SI Part 1: Chemical Syntheses of Non-Deuterated Dihydroartemisinic Acid (DHAA)

(I) The Chemical Syntheses of DHAA

The total syntheses of dihydroartemisinic acid (DHAA) (Figure S1-1, **S1-6**) from R(+)-citronellal (**S1-1**) and S(-)-isopulegol (**S1-4**) have been reported by three different research groups (Figure S1-1, Table S1-1).[1-3] These total syntheses were valuable in establishing some chemistry that was beneficial in subsequent studies that focused on the isotopically labeled DHAA compounds, which were used for mechanistic studies in the conversion of DHAA to artemisinin (see below, Table S1-1).[4-7] Two of the reports use the Robinson annulation[1,2] to form the C1-C2 and C6-C5 bonds. On the other hand, a most recent synthesis in 2016[3] uses the Grubbs RCM to form the C4-C5 bond in DHAA (**S1-6**).

1. SI Part 1: Chemical Syntheses of Non-Deuterated Dihydroartemisinic Acid (DHAA)

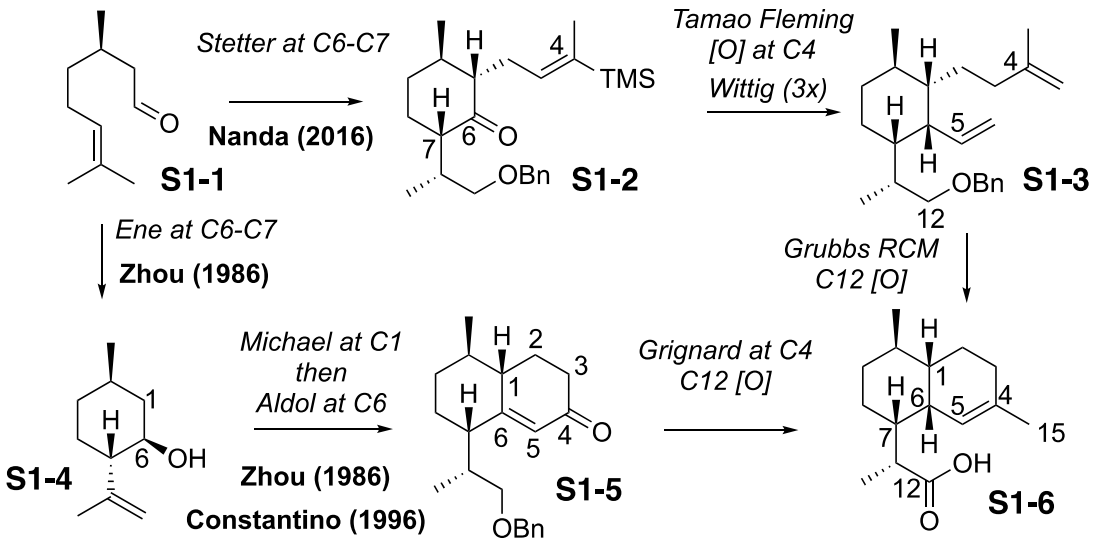

Figure S1-1. Previous reports on the chemical synthesis of DHAA (**S1-6**) from either R(+)-citronellal (**S1-1**) reported in 1986[1] and 2016[3] or S(-)-isopulegol (**S1-4**) published in 1996.[2]

Isotope incorporation has also been accomplished to yield isotopically labeled DHAA derivatives (See main text Figure 2). Deuterium was incorporated either at the C15 position[4,5,7] or the C3 position[6] of DHAA (Figure S1-1, **S1-6**).

1. SI Part 1: Chemical Syntheses of Non-Deuterated Dihydroartemisinic Acid (DHAA)

Table S1-1. Syntheses of DHAA and isotopically labeled DHAA.

Entry	Starting Material	Key Reactions
1	(R)-Citronellal[1]	Ene cyclization and Michael then aldol
2	(R)-Citronellal[3]	Stetter Reaction and Grubbs RCM
3	(-)-Isopulegol[2]	Michael reaction then aldol condensation

Synthesis of DHAA from citronellal by Xing-Xiang, X. et al. (1986)[1]

Dihydroartemisinic acid (**S1-6**) was synthesized in 14 steps from R(+)-citronellal (**S1-1**) (Figure S1-2). The synthesis began with an *ene* reaction of commercially available R(+)-citronellal **S1-1** using $ZnBr_2$. The generated alkene was then subjected to hydroboration to yield diol **S1-7**. Selective benzylation of primary alcohol **S1-7**, then subsequent oxidation of the secondary alcohol using the Jones reagent gave ketone **S1-8**. Ketone **S1-8** underwent a Michael reaction with silylated vinyl ketone, followed by simultaneous trimethyl silyl group cleavage to produce methyl ketone **S1-9**. Cyclization of methyl ketone **S1-9** with barium hydroxide octahydrate through an intramolecular aldol condensation, then dehydration with oxalic acid resulted in the desired cyclic unsaturated ketone **S1-5**. Reduction of unsaturated ketone **S1-5** with $NaBH_4$ in pyridine, followed by oxidation with Jones reagent afforded ketone **S1-10**. Methylation of ketone **S1-10** with CH_3MgI followed by dehydration with p-TsOH resulted in a 1:1 mixture of the desired dehydration product **S1-11** and its isomer which were separated by repeated flash chromatography. The pure, desired isomer **S1-11** was then treated with Na, liquid NH_3, and then oxidized with Jones reagent to yield dihydroartemisinic acid **S1-6** and its regioisomer **S1-12** in a 1:1 mixture that were separated using flash chromatography.

1. SI Part 1: Chemical Syntheses of Non-Deuterated Dihydroartemisinic Acid (DHAA)

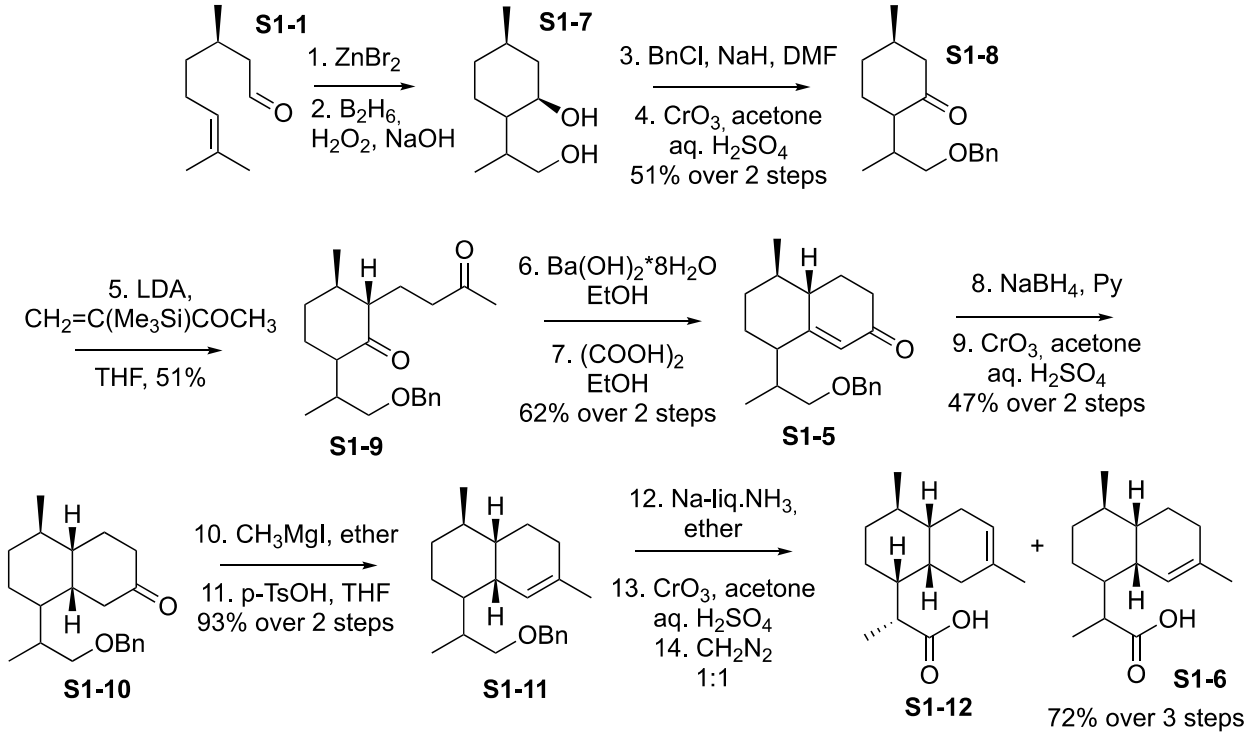

Figure S1-2. Synthesis of dihydroartemisinic acid (DHAA) (**S1-6**) from (+)-citronellal (**S1-1**) reported by Xing-Xiang and co-workers in 1986.[1] Key reactions involved an ene cyclization to form the first 6-membered ring, and a Michael reaction and aldol condensation (net Robinson annulation) to form the second 6-membered ring.

1. SI Part 1: Chemical Syntheses of Non-Deuterated Dihydroartemisinic Acid (DHAA)

Synthesis of DHAA from isopulegol by Constantino et al. (1996)[2]

Dihydroartemisinic acid (**S1-6**) was synthesized in 10 steps from commercially available S(-)-isopulegol (Figure S1-3). S(-)-Isopulegol (**S1-4**) was subjected to hydroboration which resulted in a 7:1 mixture of epimers (**S1-7a and b**) that were separated by column chromatography. Benzylation of the resulting diol **S1-7a and b** resulted in a separable mixture of isomers with the primary **S1-8a** or secondary alcohol **S1-8b** protected with a benzyl ester. The desired isomer was oxidized with pyridinium dichromate to yield ketone **S1-8**. A Robinson annulation using LDA and silylated vinyl ketone, followed by simultaneous trimethyl silyl group cleavage produced methyl ketone **S1-9**. Methyl ketone **S1-9** was cyclized with barium hydroxide octahydrate, then dehydrated with oxalic acid, resulting in α,β–unsaturated ketone **S1-5**, similar to the prior report in 1986. Pd-catalyzed hydrogenation of α,β–unsaturated ketone **S1-5** gave a separable mixture of cis- (**S1-13b**) and trans- (**S1-13a**) decalin diastereomers, with the desired cis-fused ring (**S1-13b**) being the major isomer. The cis-isomer **S1-13b** was carried forward and oxidized with pyridinium dichromate to keto-acid **S1-14**, which was then treated with MeLi to afford a mixture of C4-epimeric tertiary alcohols **S1-15**. The mixture of tertiary alcohols **S1-15** was then treated with *p*-toluenesulfonic acid to produce dihydroartemisinic acid (**S1-6**) and its Δ^3-regioisomer.

1. SI Part 1: Chemical Syntheses of Non-Deuterated Dihydroartemisinic Acid (DHAA)

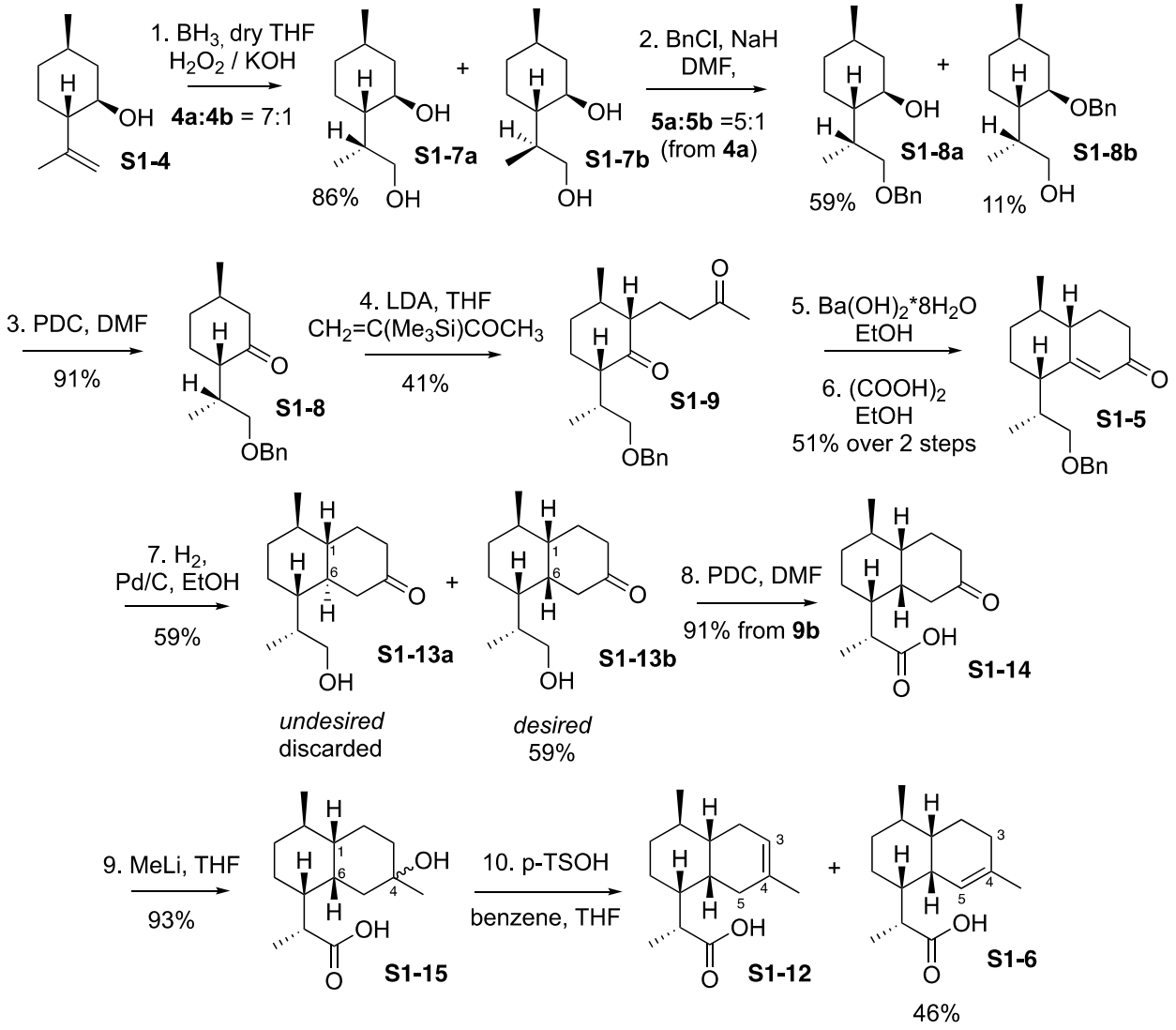

Figure S1-3. Synthesis of DHAA (**S1-6**) from S(-)-isopulegol (**S1-4**) reported in 1996[2] by Constantino and colleagues.

1. SI Part 1: Chemical Syntheses of Non-Deuterated Dihydroartemisinic Acid (DHAA)

In comparing these early synthetic strategies to dihydroartemisinic acid (**S1-6**), Constantino et al. synthesis[1] is shorter due to the early deprotection of the benzyl ester. Xing-Xiang et al.[1] does not include any isomeric mixtures until the last few steps. Both syntheses begin with the cyclized 6-membered ring (Figure S1-2, **S1-7** and Figure S1-3, **S1-4**) that is subjected to hydroboration to generate a diol and used selective benzylation on the primary alcohol (Figure S1-2, **S1-8** and Figure S1-3, **S1-8a** and **b**). They also eventually perform a Robinson annulation with the silylated vinyl ketone, then oxidized to an α,β−unsaturated ketone (Figure S1-2, **S1-5** and Figure S1-3, **S1-5**). In choosing to use Pd-catalyzed hydrogenation, Constantino et al.[2] synthesis resulted in a mixture of *cis*- and *trans*- decalin rings (Figure S1-3, **S1-13a** and **b**) (and hydrogenation of the benzyl group) which were separated using column chromatography, rather than with $NaBH_4$[1] which produced the mostly the desired *cis*-decalin ring (Figure S1-2, **S1-**10) through recrystallization with the benzyl-protected carboxylic acid still intact. To generate dihydroartemisinic acid (**S1-6**), both groups used MeLi and *p*-TsOH, resulting in dihydroartemisinic acid (**S1-6**) and it regioisomers (**S1-12**) (Figure S1-3).

1. SI Part 1: Chemical Syntheses of Non-Deuterated Dihydroartemisinic Acid (DHAA)

Synthesis of DHAA from citronellal by Rej et al. (2016)[3]

Dihydroartemisinic acid (**S1-6**) was synthesized in 13 steps[3] from R-(+)-citronellal (**S1-1**) (Figure S1-4). Using an olefin cross-metathesis with Grubbs 2nd generation catalyst and ethyl methacrylate, R-(+)-citronellal (**S1-1**) was converted to the desired α,β–unsaturated ester **S1-16**. From ester **S1-16**, an intramolecular Stetter reaction was accomplished with both a thiazolium catalyst and the Rovis catalyst to generate cyclic ketone **S1-17**. Ketone **S1-17** was reduced to a diol with $LiAlH_4$, then the resulting primary alcohol underwent selective benzylation, and the secondary alcohol was re-oxidized to ketone **S1-17** with Dess-Martin periodinane. From ketone **S1-17**, an α-homoallyl carbon chain was then installed using a kinetic enolate formation with LDA, Et_2Zn, and addition of the Stork-Jung iodide compound to produce the alkylated product **S1-18**. The resulting vinyl silane **S1-18** was treated with *m*-CPBA, yielding diketone **S1-9**. Diketone **S1-9** underwent a regioselective Wittig olefination with methyl triphenylphosphine ylide to produce keto-olefin **S1-19**, then was subjected to another Wittig reaction with methoxymethyl triphenylphosphine ylide, followed by hydrolysis with trichloroacetic acid to afford aldehyde **S1-20**. Aldehyde **S1-20** was then treated with another portion of methyl triphenylphosphine ylide to afford diene **S1-21**. Using Grubbs 2nd generation catalyst, a ring-closing metathesis was performed on diene **S1-21** to yield the bicyclic core of dihydroartemisinic acid **S1-11**. The synthesis of dihydroartemisinic acid (**S1-6**) was then completed following the final two steps of Zhou et al. synthesis with reduction of the benzyl ester using Na and liquid NH_3, followed by oxidation with Jones reagent to produce dihydroartemisinic acid (**S1-6**).

1. SI Part 1: Chemical Syntheses of Non-Deuterated Dihydroartemisinic Acid (DHAA)

1. SI Part 1: Chemical Syntheses of Non-Deuterated Dihydroartemisinic Acid (DHAA)

Although this synthesis[2] is longer, it uses new chemistry beginning from R(+)-citronellal (S1-1). Avoiding the *ene* cyclization with $ZnBr_2$, Rej, R. K. et al. instead chose to carry out a olefin cross-metathesis with ethyl methacrylate and Grubbs 2nd generation catalyst. Using asymmetric catalysis and an intramolecular Stetter reaction, they were able to generate the 6-membered ring without any isomeric mixtures. This is advantage over the previous two synthesis[1,3] to avoid extra chromatography separations and ensure correct stereochemistry of the molecule. Rej, R. K. et al.[3] chose to use selective benzylation as in the other syntheses,[1,2] and oxidized with the milder reagent, Dess-martin periodinane, rather than using Jones reagent[1] or PDC.[2] To alkylate ketone, Rej et al.[3] also used a Robinson Annulation,[1] however, instead of using the silylated vinyl ketone, they used the Stork-Jung iodide reagent.[3] Use of Wittig reagents to generate a diene intermediate that could be closed using a Grubbs ring closing metathesis reaction was also unique to this procedure, rather than the use of barium hydroxide octahydrate[1,2] to cyclize. The final steps used to synthesize dihydroartemisinic acid (**S1-6**) by Rej et al.[3] followed Xing-Xiang, X. et al. procedure[1] to deprotect the benzyl ester using Na and liquid ammonia, then oxidizing to the carboxylic acid using Jones reagent.

1. SI Part 1: Chemical Syntheses of Non-Deuterated Dihydroartemisinic Acid (DHAA)

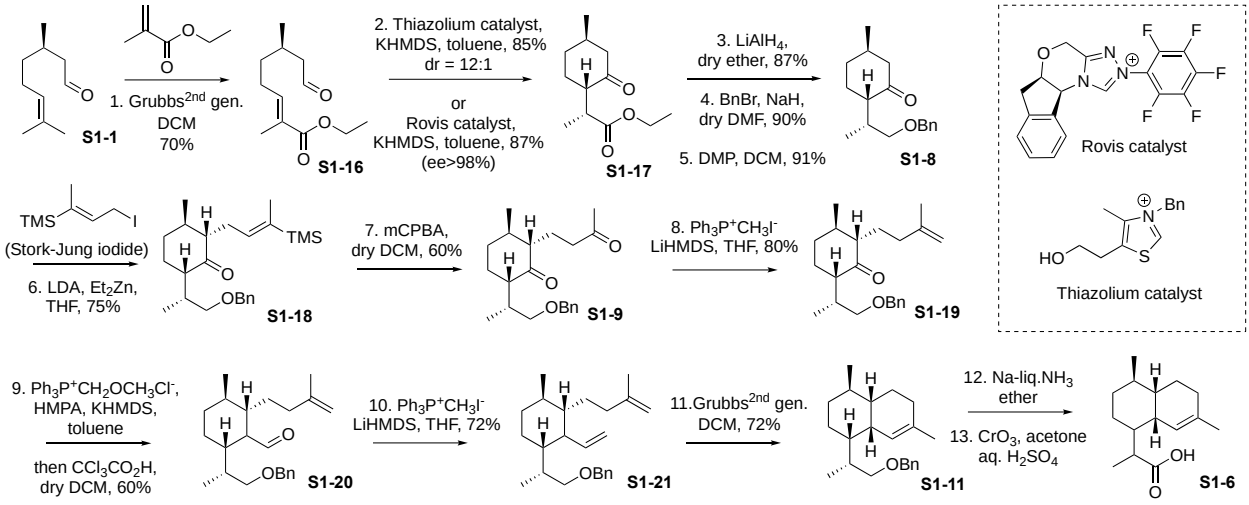

Figure S1-4. Synthesis of DHAA (**S1-6**) from R(+)-citronellal (**S1-1**) using a Stetter reaction to form the C6-C7 bond and later a Grubbs ring closing metathesis to form the C4-C5 double bond of the cis-dehydrodecalin ring of DHAA.[3]

Dihydroartemisinic acid (**S1-6**) can also be synthesized from amorpha-4,11-diene (**S1-22**) (Figure S1-5).[8] Selective boration of the C11 double bond resulted in primarily (R)-epimer alcohol (**S1-23**), followed by oxidation to aldehyde **S1-24** with SO_3 pyridine complex, then oxidation to dihydroartemisinic acid (**S1-6**) using NaOCl.

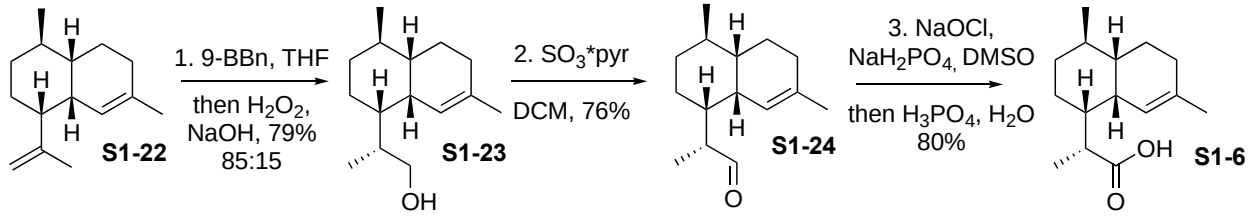

Figure S1-5. Synthesis of DHAA (**S1-6**) from amorpha-4,11-diene (**S1-22**).[8]

1. SI Part 1: Chemical Syntheses of Non-Deuterated Dihydroartemisinic Acid (DHAA)

Bhonsle et al. 1994[9] and Yadav et al. 2010[10] also synthesized dihydroartemisinic acid analogs in their synthesis toward artemisinin (schemes shown in Wang et al. 2014,[11] Zhu and Cook 2014,[12] respectively).

Beginning from amorpha-4,11-diene (**S1-25**) (Figure S1-6), Keasling's group (2009)[12] used native *Artemisia annua* cytochrome P450 monooxygenase (CYP71AV1/ $P450_{AMO}$) and an engineered prokaryotic cytochrome P450 ($P450_{BM3}$) from *Bacillus megaterium* to synthesize dihydroartemisinic acid (**S1-6**). $P450_{BM3}$ epoxidizes amorpha-4,11-diene (**S1-25**) to artemisinic-11S,12-epoxide (**S1-26**), then can be reduced to dihydroartemisinic alcohol **S1-23** using sodium cyanoborohydride. Oxidation of dihydroartemisinic alcohol **S1-23** to an aldehyde, then carboxylic acid produces dihydroartemisinic acid **S1-6**. This epoxidation of amorphadiene **S1-25** by $P450_{BM3}$ is in contrast to the use of $P450_{AMO}$ (P450 71AV1 from *Artemisia annua*) which is required to be used from amorpha-4,11-diene in 3 separate steps to produce artemisinic acid **S1-27**, which is then reduced to dihydroartemisinic acid (**S1-6**).

1. SI Part 1: Chemical Syntheses of Non-Deuterated Dihydroartemisinic Acid (DHAA)

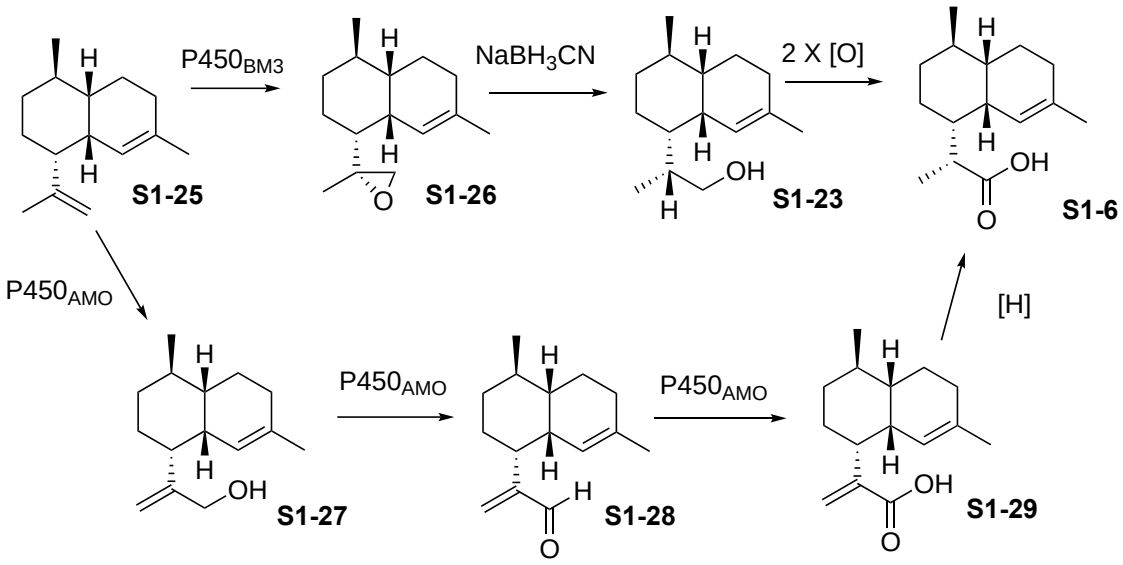

Figure S1-6. Synthesis of dihydroartemisinic acid (**S1-6**) from amorphadiene (**S1-25**) using $P450_{BM3}$ or $P450_{AMO}$.[12]

2. SI Part 2: Biosynthesis of Dihydroartemisinic Acid

(II) The Biosynthesis of DHAA

Dihydroartemisinic Acid (DHAA) Biosynthesis – Farnesyl Pyrophosphate (FPP) Biosynthesis

With respect to its biosynthesis of dihydroartemisinic acid (Figure S1-1, **S1-6**), many efforts have been focused on understanding its formation and the topic has been reviewed by others.[13-18] Here, we briefly summarize the pathway in this section. The most fundamental carbon backbone of artemisinin begins with acetylCoA (Figure S2-1, **S2-1**),[19] which undergoes 9 biosynthetic steps via the mevalonate pathway (Figure 16. The enzymes involved in the mevalonate pathway (9 steps) include: ERG10, ERG13, tHMGR, ERG12, ERG8, ERG19, IDI1, ERG20, ERG20) to farnesyl diphosphate[20] (FPP) (**S2-11**),[21-24] which is the precursor to amorphadiene (Figure S2-3, **S2-22**). As an alternative to the mevalonate pathway to FPP, the deoxy-D-xylulose-5-phosphate (DXP) pathway (Figure S2-2) from pyruvate (**S2-12**) and glyceraldehyde-3-phosphate (**S2-13**)[25] exists 8 steps catalyzed by the following enzymes: dxs, ispC, ispD, ispE, ispF, ispG, ispH, and idi).

2. SI Part 2: Biosynthesis of Dihydroartemisinic Acid

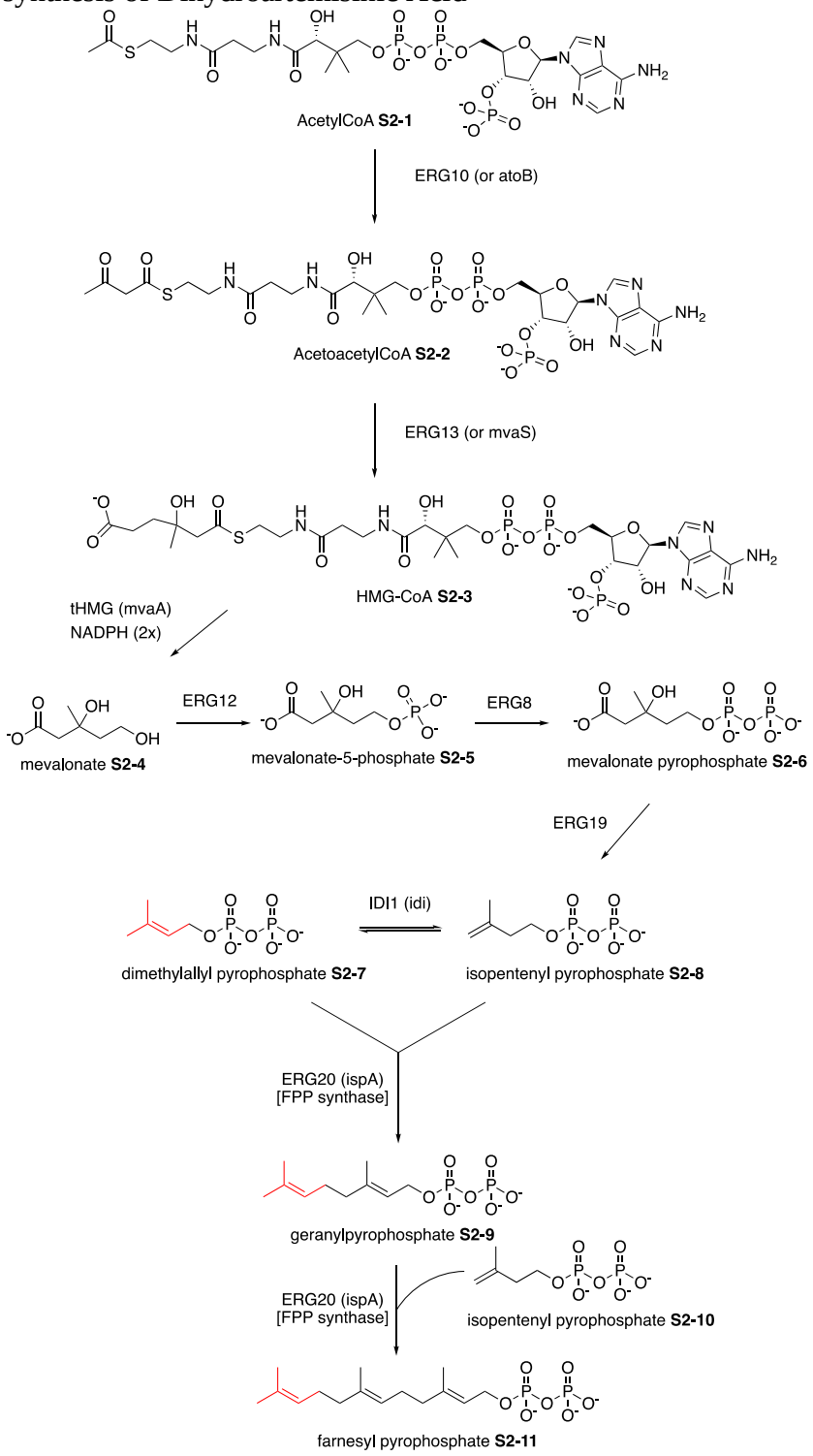

Figure S2-1. The mevalonate pathway (9 biosynthetic steps) from acetyl-CoA (**S2-1**) to farnesylpyrophosphate (FPP) (**S2-11**), the direct biosynthetic precursor of amorphadiene **S2-22**. Enzymes in parentheses are the ones from bacteria, while the enzymes not in parentheses are from fungi (*Saccharomyces cerevisiae*[26]).[27]

2. SI Part 2: Biosynthesis of Dihydroartemisinic Acid

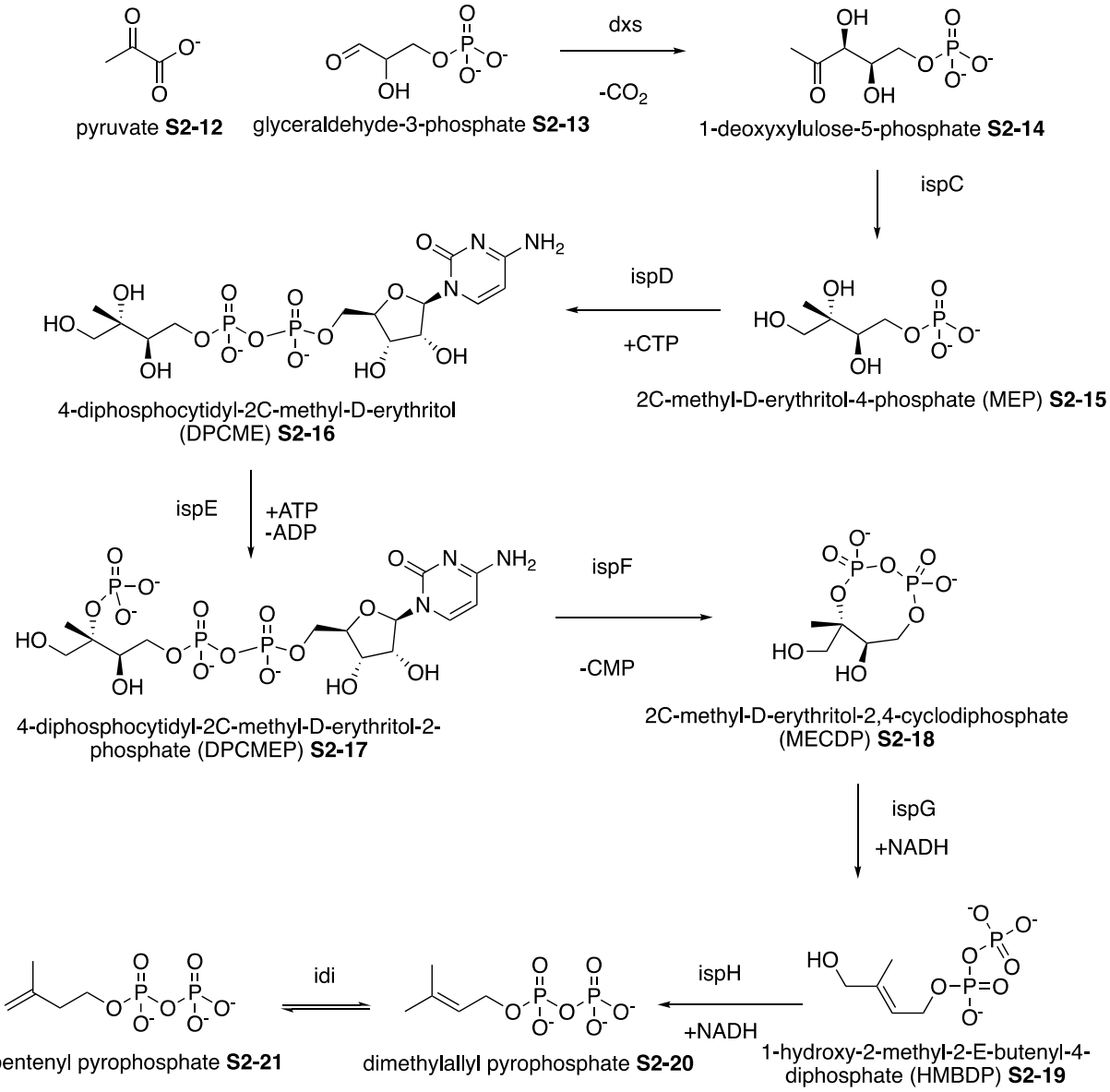

Figure S2-2. The DXP pathway from pyruvate (**S2-12**) and glyceraldehyde-3-phosphate (**S2-13**) to dimethylallyl pyrophosphate (**S2-20**) and isopentenyl pyrophosphate (**S2-21**),[28] which lead to the formation of FPP (**S2-11**) (see Figure S2-1).

2. SI Part 2: Biosynthesis of Dihydroartemisinic Acid

Five Enzymes that Convert Dihydroartemisinic Acid (DHAA) Biosynthesis from FPP

Once farnesyl pyrophosphate (Figure S2-2, **S2-11**) is biosynthesized in cells, the plant enzymes from *Artemisia annua* lead to the formation of dihydroartemisinic acid (DHAA) (Figure S2-3, **S2-26**) through five different enzymes (Figure S2-3 and Table S2-1). The enzymes from amorphadiene (**S2-22**) to DHAA (**S2-26**) have previously been identified and confirmed through heterologous expression in a yeast system [29-33] and bacteria.[34] In the yeast microsome system, the main limitation of the previous studies was the lack of the use of purified enzymes, resulting in background enzymatic activity of the host organism (yeast).

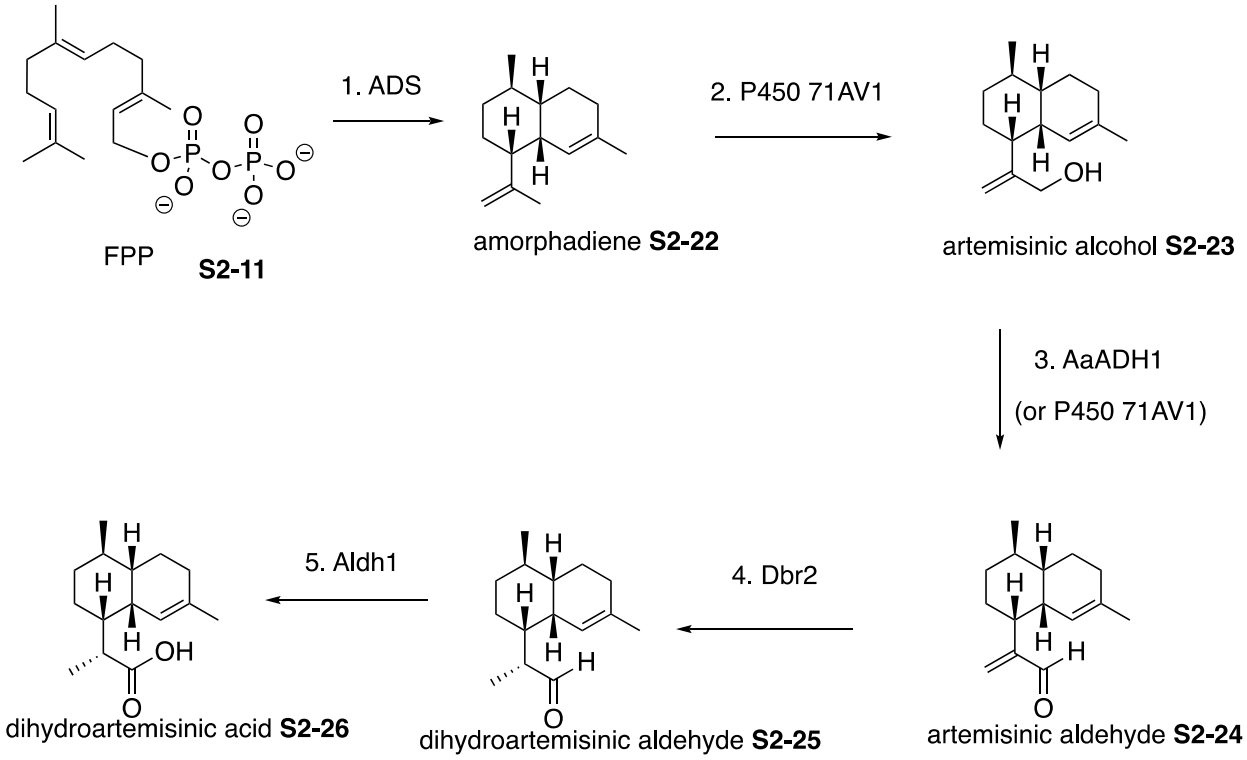

Figure S2-3. FPP (**S2-11**) is converted to dihydroartemisinic acid (DHAA) (**S2-26**), the biosynthetic precursor of artemisinin, through five enzymes: amorphadiene synthase (ADS), cytochrome P450 71AV1 (P450 71AV1), *A. annua* alcohol dehydrogenase 1 (AaADH1), double bond reductase (DBR), and dihydroartemisinic aldehyde dehydrogenase (AldH).

2. SI Part 2: Biosynthesis of Dihydroartemisinic Acid

Table S2-1. The five enzymes that convert FPP (**S2-11**) to DHAA (**S2-26**) from *Artemisia annua*.

Entry	Enzyme	Reaction	Accession
1	ADS[8,35-38]	FPP to Amorphadiene	Q9AR04.2
2	P450 71AV1[39]	Amorphadiene to Artemisinic Alcohol	Q1PS23.2
3	AaADH1[40]	Artemisinic Alcohol to Artemisinic Aldehyde	PWA47650.**1**
4	DBR[41]	Artemisinic Aldehyde to Dihydroartemisinic Aldehyde	C5H429.2
5	Aldh1[42]	Dihydroartemisinic Aldehyde to DHAA	C5I9X1.1

Step 1 of 5 (FPP to DHAA): Amorphadiene Synthase (ADS) Converts FPP to Amorphadiene \

Amorphadiene **S2-22** is formed from FPP **S2-11** through amorphadiene synthase (ADS),[43] a class I terpenoid synthase consisting of 546 amino acid residues (Figure S2-4).[35] The mechanism of ADS in the conversion of FPP **S2-11** to amorphadiene **S2-22** has been studied extensively[37,44] and can be described by the following steps: (i) rearrangement of the phosphate from C1 to C3 **S2-27**, (ii) formation of the allylic carbocation **S2-28** at C1, (iii) 1,6-cyclization to form the bisabolyl cation **S2-29**, (iv) 1,3-hydride shift to form the allylic carbocation at C1 **S2-30**, (v) 1,10-cyclization to form the second 6-membered ring **S2-31**, and (vi) deprotonation to form the C11-C12 double bond of amorphadiene (**S2-22**). The crystal structure of amorphadiene synthase has not been reported, but several studies have used homology models to rationalize the mechanism of this enzyme.[36,45]

2. SI Part 2: Biosynthesis of Dihydroartemisinic Acid

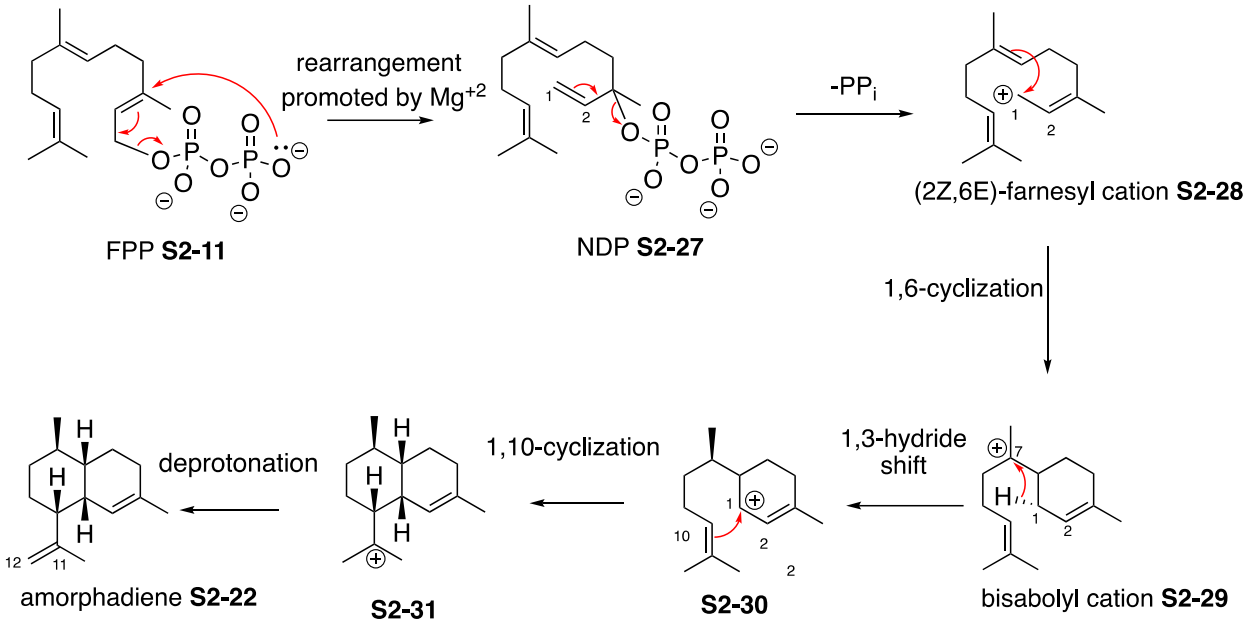

Figure S2-4. Mechanism of FPP **S2-11** to amorphadiene **S2-22** by amorphadiene synthase (ADS).[35]

2. SI Part 2: Biosynthesis of Dihydroartemisinic Acid

Step 2 of 5 (FPP to DHAA): P450 71AV1 oxidation of amorphadiene to artemisinic alcohol

Cytochrome P450 71AV1 was identified as the responsible enzyme to oxidize the allylic C13-position of amorphadiene **S2-22** to yield artemisinic alcohol **S2-23** (Figure S2-5). The P450 reductase protein from *Artemisia annua*, which transfers the electrons from NADPH to the P450 protein, has previously been studied.[46]

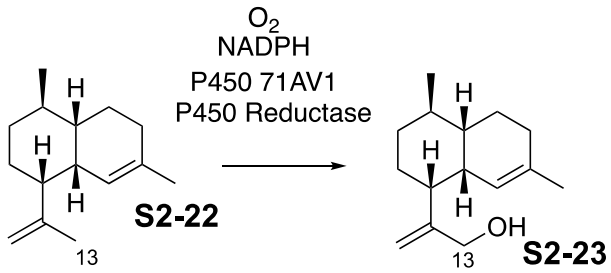

Figure S2-5. The conversion of amorphadiene **S2-22** to artemisinic alcohol **S2-23** catalyzed by P450 71AV1.

The prototypical C-H hydroxylation reaction catalyzed by cytochrome P450 enzymes undergoes a nine-step catalytic cycle (Figure S2-6). The electron transfer steps at step 2 and step 4 are provided by NADPH, which is transferred from NADPH P450 reductase one electron at a time. Kinetic isotope effects (KIEs) of human P450 enzymes using deuterated substrates have previously shown results[47] supporting partially rate-limiting nature of the C-H abstraction step (the seventh step). The oxoferryl iron species has a porphyrin cation pi radical, which is reduced after the hydrogen atom abstraction from its substrate. Plant cytochrome P450 enzymes play important roles in producing bioactive natural products.[48,49]

2. SI Part 2: Biosynthesis of Dihydroartemisinic Acid

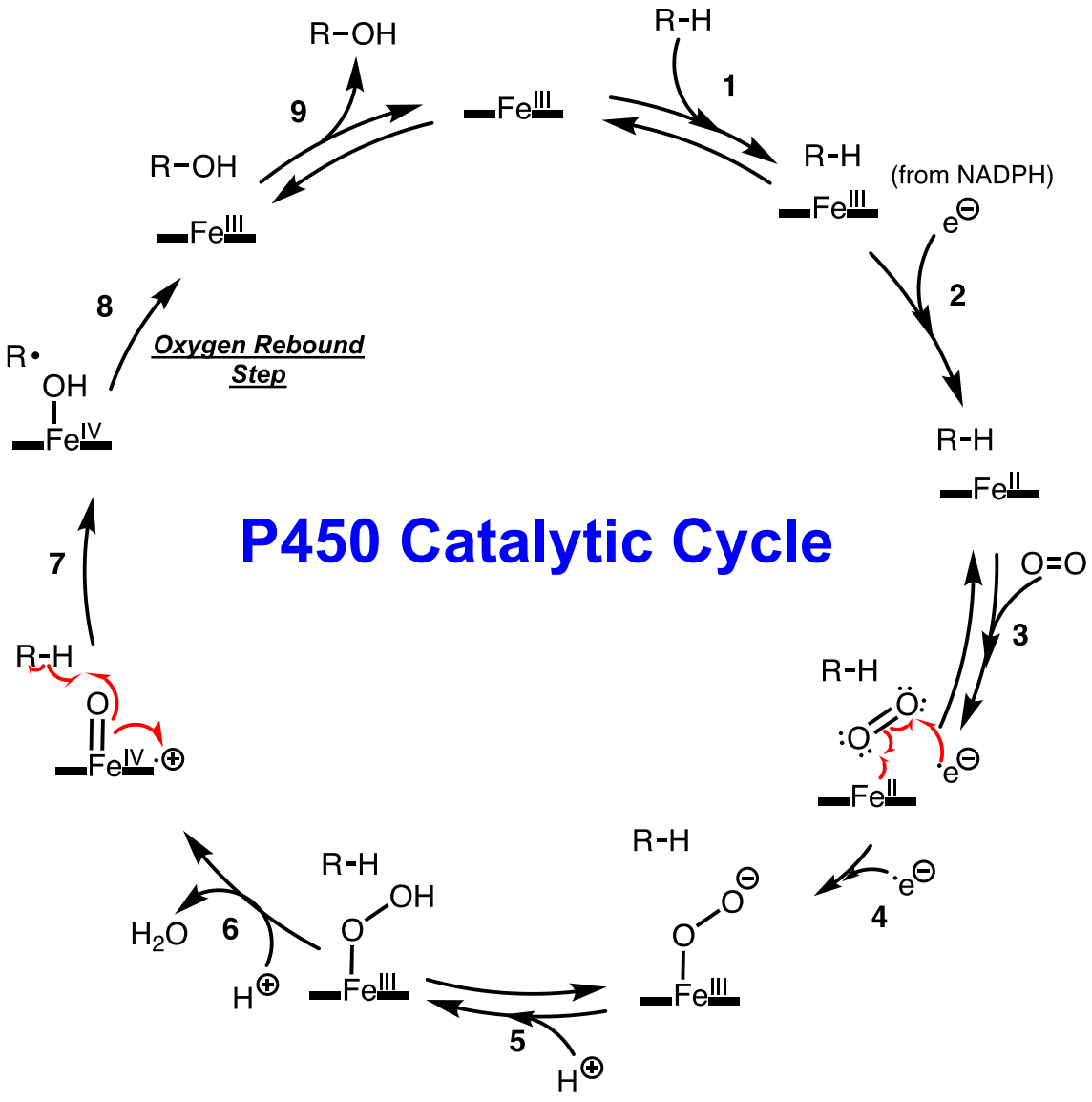

Figure S2-6. The general 9-step catalytic cycle of the prototypical C-H hydroxylation reaction of a cytochrome P450 enzyme.

2. SI Part 2: Biosynthesis of Dihydroartemisinic Acid

Step 2: P450 71AV1 oxidation of amorphadiene in 3 steps and nature of processivity?

An enzyme that catalyzes more than one step to convert its substrate into its final product can be either characterized as processive or distributive. A processive enzyme is one that catalyzes multiple steps without releasing any of the intermediates (i.e. the intermediates have high affinity for the enzyme and stays bound until it is converted to the final product).[50,51] P450 71AV1 can potentially be classified as a processive or distributive enzyme depending on whether this enzyme can oxidize amorphadiene **S2-22** to artemisinic acid **S2-29** over three hydroxylations (Figure S2-7). In order to determine the processivity of the 3-step oxidation of amorphadiene to artemisinic acid (Figure S2-7, **S2-22** to **S2-29**), pulse-chase assays are possible[51] to show if the intermediates stay bound to the P450 enzyme.[6] Enzyme incubations could begin with 3,3-d_2-amorphadiene, and at time t either add: (i) non-labeled artemisinic alcohol (first intermediate or "chase") or (ii) carrier solvent. At the second time point, reactions could be quenched and 3,3-d_2-artemisinic- alcohol, aldehyde, and acid could be determined by LC-MS. If equal amounts of 3,3-d_2-artemisinic-alcohol, aldehyde, and acid are detected in the presence and absence of the chase, then this multi-step reaction (from amorphadiene to the aldehyde to the acid (Figure S2-7, **S2-22** to **S2-29**)) is determined to be processive. On the other hand, if there were fewer d_2-oxidation products detected when a chase was added, then the reaction is distributive. Classically in P450 systems,[50,52,53] pulse-chase experiments to determine processivity usually involves a radioactive starting material, however, the use of polydeuterated and non-deuterated intermediates would be possible to enable a nonradioactive approach to distinguish between the different intermediates (i.e. pulse vs. chase). Although it was shown that P450 71AV1 could perform the sequence of three oxidations with yeast microsomes, none of the previous studies used the purified enzyme.[29,42] It would also be

interesting to test whether or not a cytochrome b_5 (b_5) effect is observed in the plant P450 enzyme systems where the presence of b_5 could promote enzymatic activity – similar to what occurs in the human P450 enzymes.

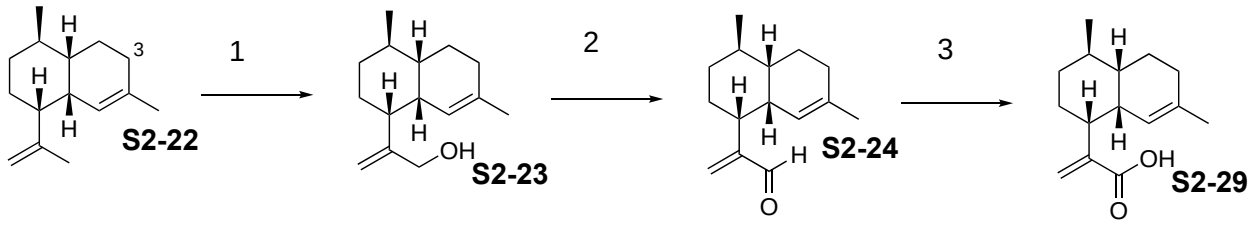

Figure S2-7. The three-step oxidation of amorphadiene **S2-22** to artemisinic acid **S2-29** catalyzed by *A. annua* P450 71AV1.

Furthermore, cytochrome b_5 (b_5) is hypothesized to promote processivity [54] and this protein could be expressed and purified to determine its effect on enhancing processivity. If b_5 promotes P450 catalysis, the interacting residues between the P450 and b_5 could be identified using crosslinking mass spectrometry. Crosslinking mass spectrometry[55] was previously employed to identify the interacting residues between human P450 17A1 and b_5.[56,57] The sequence alignment of *A. annua* P450 71AV1 with human P450 17A1 is shown in Figure S2-8. The highlighted residue in P450 17A1 (R358) corresponds to a positively charged lysine residue (K356) in *A. annua* P450 71AV1.

2. SI Part 2: Biosynthesis of Dihydroartemisinic Acid

```
Q1PS23.2      1   MKSILKAMALSLTTSIALATILLFVYKFATRSKST-KKSLPEPWRLPIIGHMHHLIG-TTPHRGVRDLARKYGSLMHLQL  78
NP_000093.1   1   MWELVALLLLTLA------------YLFWPKRRCPGAKYPKSLLSLPLVGSLPFLPRHGHMHNNFFKLQKKYGPIYSVRM  68

Q1PS23.2      79  GEVPTIVVSSPKWAKEILTTYDISFANRPETLTGEIVLYHNTDVVLAPYGEYWRQLRKICTLELLSVKKV-KSFQSLREE  157
NP_000093.1   69  GTKTTVIVGHHQLAKEVLIKKGKDFSGRPQMATLDIASNNRKGIAFADSGAHWQLHRRLAMATFALFKDGDQKLEKIICQ  148

Q1PS23.2      158 ECWNLVQEIKASGSGRPVNLSENVFKLIATILSRAAFGKGIK-DQKELTEIVK---EILRQTGGFDVADIFP-SKKFLHH  232
NP_000093.1   149 EISTLCDMLATHNGQS-IDISFPVFVAVTNVISLICFNTSYKNGDPELNVIQNYNEGIIDNLSKDSLVDLVPWLKIFPNK  227

Q1PS23.2      233 LSGKRARLTSLRKKIDNLIDNLVAEH-TVNTSSKTNETLLDVLLRLK----------DSAEFPLTSDNIKAIILDMFGA  300
NP_000093.1   228 TLEKLKSHV---KIRNDLLNKILENYKEKFRSDSITN-MLDTLMQAKMNSDNGNAGPDQDSELLSDNHILTTIGDIFGA  302

Q1PS23.2      301 GTDTSSSTIEWAISELIKCPKAMEKVQAELRKALNGKEKIHEEDIQELSYLNMVIKETLRLHPPLPLVLPRECRQPVNLA  380
NP_000093.1   303 GVETTTSVVKWTLAFLLHNPQVKKKLYEEIDQNVGFSRTPTISDRNRLLLLEATIREVLRLRPVAPMLIPHKANVDSSIG  382

Q1PS23.2      381 GYNIPNKTKLIVNVFAINRDPEYWKDAEAFIPERFENSSAT-VMGAEYEYLPFGAGRRMCPGAALGLANVQLPLANILYH  459
NP_000093.1   383 EFAVDKGTEVIINLWALHHNEKEWHQPDQFMPERFLNPAGTQLISPSVSYLPFGAGPRSCIGEILARQELFLIMAWLLQR  462

Q1PS23.2      460 FNWKLPNGVSYDQIDMTESSG-ATMQRKTELLLVP----------SF  495 A. annua P450 71AV1
NP_000093.1   463 FDLEVPDD---GQLPSLEGIPKVVFLIDSFKVKIKVRQAWREAQAEGST  508 Human P450 17A1
```

Figure S2-8. Multiple sequence alignment between Artemisia annua P450 71AV1 and human P450 17A1.

2. SI Part 2: Biosynthesis of Dihydroartemisinic Acid

Conversion of artemisinic aldehyde to artemisinic acid by P450 71AV1 (Ferric Peroxide vs. Compound I)

One interesting chemical reaction catalyzed by P450 71AV1 is the oxidation of the aldehyde **S2-24** to the carboxylic acid **S2-31** (Figure S2-9). Two distinct mechanisms can be proposed that involve either a ferric peroxide intermediate (Figure S2-9A) or a Compound I mechanism (Figure S2-9B). The gem-diol to aldehyde equilibrium in water will be determined for artemisinic aldehyde (Figure S2-9B). In a separate incubation, P450 71AV1 will be incubated with artemisinic aldehyde in the presence of $^{18}O_2$. In the ferric peroxide mechanism, an ^{18}O atom is guaranteed to be incorporated into the carboxylic acid product while in the Compound I mechanism, a mixture of isotopologues containing one ^{18}O atom and no ^{18}O atom is obtained and their ratio could depend on the equilibrium of the *gem*-diol and the aldehyde in water. Based on previous studies with human cytochrome P450 19A1 aromatase,[58] we hypothesize that Compound I is the operative active iron intermediate in the oxidation of the aldehyde substrate to the carboxylic acid product. However, recent efforts to mechanistically elucidate the active iron species in cytochrome P450 enzymes have revealed that ferric peroxide is a viable active form that catalyzes reaxtions.[59,60]

2. SI Part 2: Biosynthesis of Dihydroartemisinic Acid

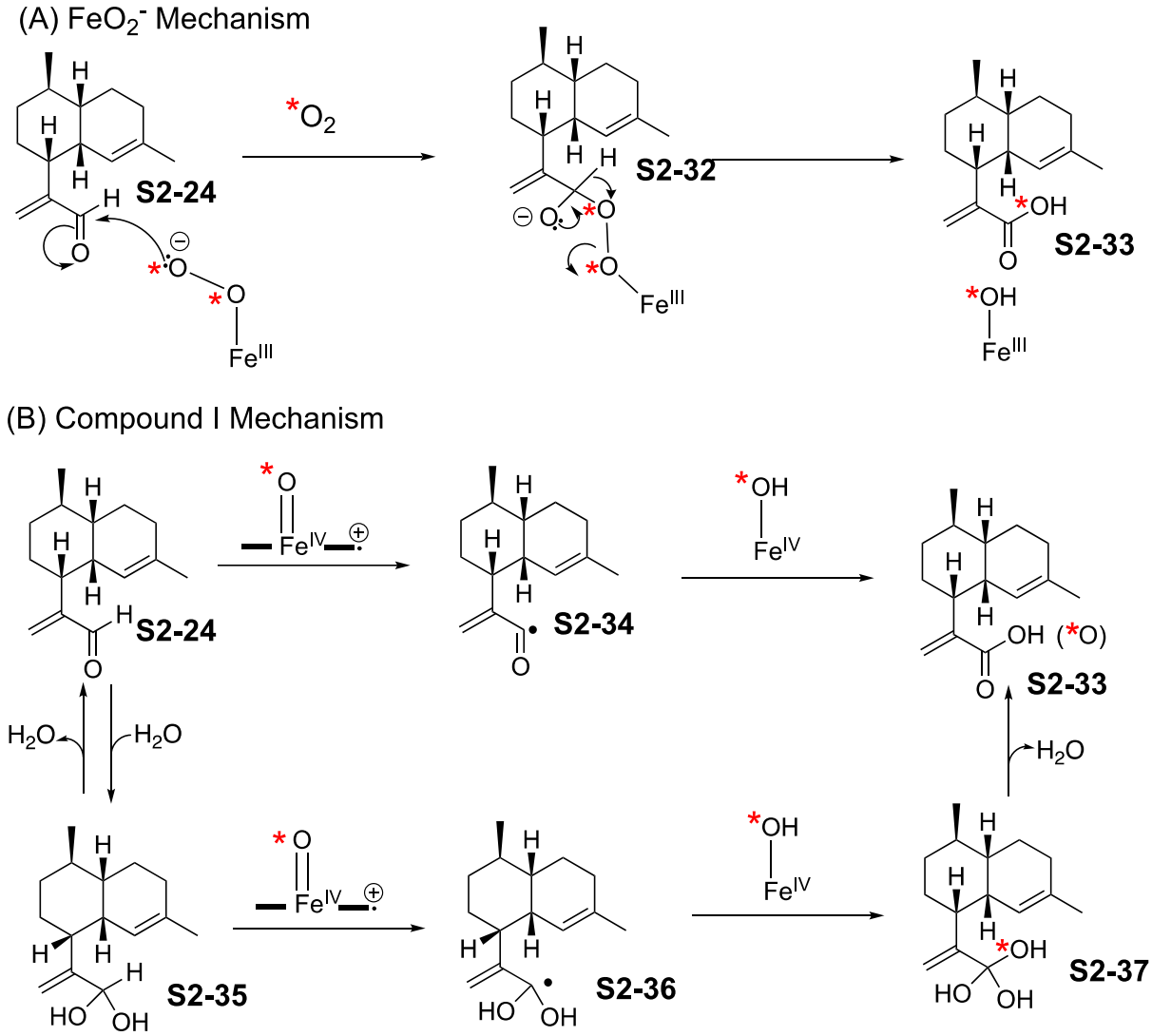

Figure S2-9. Two mechanisms are proposed for the conversion of artemisinic aldehyde **S2-24** to artemisinic acid **S2-31**. The mechanism could be determined from $^{18}O_2$ labeling studies. *O_2 = $^{18}O_2$.

2. SI Part 2: Biosynthesis of Dihydroartemisinic Acid

Step 3 of 5 (FPP to DHAA): Alcohol dehydrogenase that converts artemisinic alcohol to artemisinic aldehyde

The third step from FPP (**S2-11**) to DHAA (**S2-26**) (Figure S2-3) involves the oxidation of the P450 71AV1 product, artemisinic alcohol **S2-23**, to artemisinic aldehyde **S2-24**, by alcohol dehydrogenase 1 from *Artemisia annua* (AaDH1) (Figure S2-10). Furthermore, the crystal structure of *Artemisia annua* alcohol dehydrogenase 1 has been solved where the enzyme is bound to NAD^+ (PDB ID: 6LJH and 7CYI).[40] Another alcohol dehydrogenase from *Artemisia annua* (ADH2) has been previously reported, however, in this study, none of the substrates tested against this enzyme included artemisinic alcohol (instead, artemisia alcohol was used).[33]

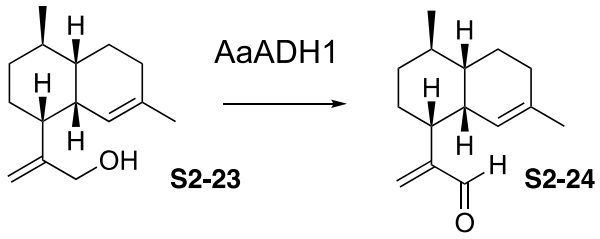

Figure S2-10. The oxidation of artemisinic alcohol **S2-23** to artemisinic aldehyde **S2-24** reportedly catalyzed by AaADH1.

2. SI Part 2: Biosynthesis of Dihydroartemisinic Acid

Step 4 of 5 (FPP to DHAA): Double bond reductase-2 (DBR-2) converts artemisinic aldehyde to dihydroartemisinic aldehyde

An N-terminal hexahistidine-tagged artemisinic aldehyde Δ11(13) reductase has been previously expressed and purified.[32] The authors in this study used 1 mM NADPH as the source of the stoichiometric reductant. The limitation in this study was that the only substrate tested for this enzyme in artemisinin biosynthesis was dihydroartemisinic aldehyde (Figure S2-11, **S2-24** to **S2-25**). However, there are other α,β-unsaturated carbonyl derivatives found in artemisinin biosynthesis (i.e. artemisinic acid and artemisitene), and it would be worthwhile to re-examine this enzyme's activity on these other potential substrates to reveal alternative pathways to artemisinin. Artemisinic acid could also be converted to artemisitene using the autoxidation method we developed for dihydroartemisinic acid to artemisinin.[6] As an alternative biosynthetic route to artemisinin, artemisitene could in turn be reduced by double bond reductase to yield artemisinin.

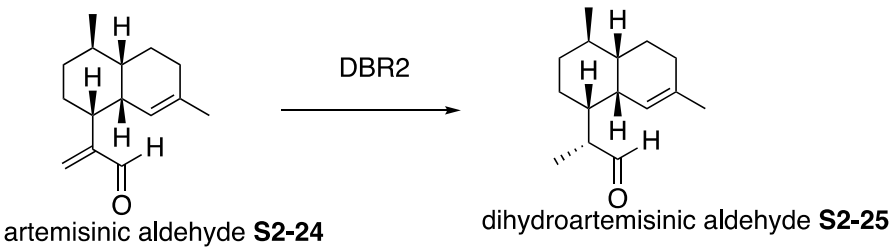

Figure S2-11. The reduction of artemisinic aldehyde **S2-24** to dihydroartemisinic aldehyde **S2-25** catalyzed by double bond reductase (DBR2).

2. SI Part 2: Biosynthesis of Dihydroartemisinic Acid

Step 5 of 5 (FPP (S2-11) to DHAA (1)): Artemisinic aldehyde dehydrogenase converts dihydroartemisinic aldehyde S2-25 to dihydroartemisinic acid (1)

In Figure S2-12 , the mechanism for oxidation of dihydroartemisinic aldehyde (**S2-12**) to dihydroartemisinic acid (**S2-26**) is proposed for aldehyde dehydrogenase. Previous studies have identified an aldehyde dehydrogenase responsible in converting dihydroartemisinic aldehyde (**S2-12**) to dihydroartemisinic acid (**S2-26**).[42] This reaction requires NAD as the oxidant.

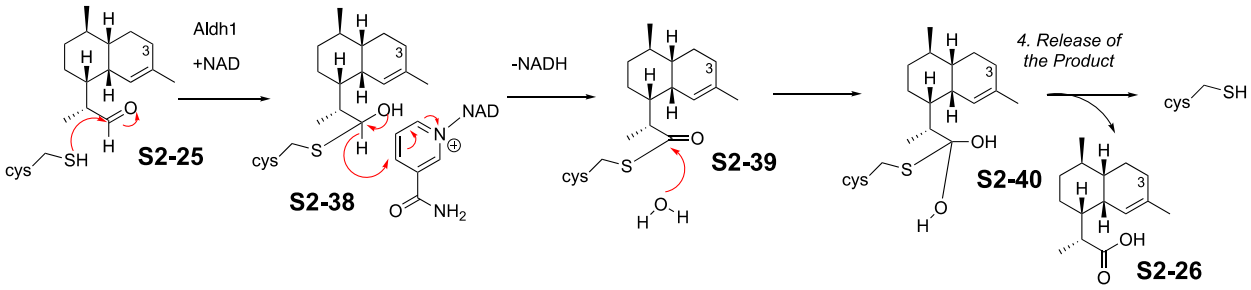

Figure S2-12. The mechanism of conversion of dihydroartemisinic aldehyde **S2-25** to dihydroartemisinic acid **S2-26** by aldehyde dehydrogenase (Aldh1).

3. SI Part 3: Analytical Techniques to Detect DHAA and Artemisinin

In Acton and Roth's study in 1992, they used GC/MS (EI) obtained from a Hewlett Packard 5890 GC with a 5970 mass selective detector and CIMS (NH_3) from a Nermag R 10-10C spectrometer were used to analyze products of dihydroartemisinic acid hydroperoxide and dihydroartemisinic acid exposed to $^{18}O_2$ in petroleum ether and TFA.

In 2001, Sy, Zhu, and Brown used ^{1}H and ^{13}C NMR data with 2D-NMR techniques (HSQC, HMBC, COSY) of their isolated natural products from *Artemisia annua*. For their labelled isotopomers of dihydroartemisinic acid, they relied on ^{13}C NMR signals and splitting patterns. HR-MS in EI mode at 70 eV on a Finnigan-Mat 95 MS spectrometer (not specified if GC or LC) was used to analyze the molecular ions and daughter ions formed by the fragmentation of the $^{2}H_3$-labelled dihydroartemisinic isotopomers, but they pointed out inaccuracies in the mass spectral analysis due to additional peaks caused by hydrogen/deuterium loss. The other high resolution data for the other synthesized isotopomers were not stated and the raw spectra were not provided.

Artemisinin has an infrared spectrum with intense peaks at 1745 cm^{-1} for its δ-lactone, and peaks at 831, 881, 1115 cm^{-1} for the peroxide functional group.[61]

3. SI Part 3: Analytical Techniques to Detect DHAA and Artemisinin

Since NMR signals were an important tool in these studies, it is important to indicate the diagnostic signals of artemisinin. The ^{1}H-NMR assignment of artemisinin contains 3 methyl substituents, (**3-Me**- δ 1.44 singlet, **6-Me**- δ 0.99 doublet, and **9-Me**- δ 1.21 doublet). The hydrogen between the 7-membered ring and lactone (**12**) is the most diagnostic proton with a ^{1}H signal of a δ5.87 singlet. The ^{13}C-NMR assignments of the three methyl groups are **3-Me**- δ 25.10, **6-Me**- δ 19.74, and **9-Me**- δ 12.47. The lactone carbon (**10**) has a ^{13}C signal at δ 171.92. Carbon **12a** and **3** are downfield at δ 79.38 and δ 105.22 respectively, as well as carbon **12** at δ 93.62 because of their proximity to the oxygen atoms of the endoperoxide ring and lactone.[62]

Sy and Brown 2002 mainly used ^{1}H and ^{13}C NMR data to report 'isolated' intermediates from a $CDCl_3$ solution of dihydroartemisinic acid kept in an NMR tube and monitored over 7 months.[63] Using comparison with previous ^{1}H NMR data reported in literature, they identified dihydroartemisinic acid hydroperoxide, dihydro-*epi*-deoxyarteannuin B, and arteannuin H. For characterization of some of the intermediates, they again used HR-EIMS at 70 eV on a Finnigan-Mat 95 MS spectrometer.

3. SI Part 3: Analytical Techniques to Detect DHAA and Artemisinin

In both of our 2020 and 2021 studies,[6,7] time courses were carried out using ^{1}H NMR spectroscopy analyzed with Topspin software and HRMS data was acquired on a LTQ Orbitrap XL connected to a Waters Acquity UPLC system and analyzed with Qualbrowser software. ^{2}H NMR was used to show incorporation of deuterium in synthesized deuterated dihydroartemisnic acid isotopologues. A new method was developed to quantify the spontaneous conversion of dihydroartemisinic acid to artemisinin using an internal standard and the integrations under the curve of masses analyzed. Similar to Acton and Roth, and Brown and Sy, electrospray ionization (ESI) was used. ESI allows for good sensitivity (fmol – pmol), a practical mass range of up to 70,000 Da, and it is the softest ionization method (Siuzdak, 2005).[64] We used both ESI- positive and negative mode, and found the best mode was positive to detect dihydroartemisinic acid and artemisinin. The advantage of the LTQ Orbitrap was the distinction between the ^{13}C-abundant isotope mass (m/z 284.1574) signal and the deuterated artemisinin isotopologue mass signal (m/z 283.1540) which required ~100,000 mass resolution.

3. SI Part 3: Analytical Techniques to Detect DHAA and Artemisinin

Artemisinin does not show up on LC-HRMS negative mode because it cannot ionize (i.e. there is no functional group that can form a negative charge) while DHAA forms a negative carboxylate anion. In positive mode, artemisinin has an exact mass of *m/z* 283.1540. For dihydroartemisinic acid, is ionizes and presents the best signal in negative mode, with primarily one mass of 235.1704. In positive mode, dihydroartemisinic acid displays two mass signals at *m/z* 237.1849 for protonated dihydroartemisinic acid, and dihydroartemisinic acid carbocation (*m/z* 235.1693). This was shown to occur when 3,3-$^{2}H_2$-dihydroartemisinic acid resulted in the mass spectrum including the protonated d_3-isotopologue *m/z* 240.2037, and carbocation of the d_3-isotopologue *m/z* 238.1881. Within the ionization source, the d_3-isotopologue lost a deuterium atom and a mass of *m/z* 237.1818 was detected as the d_2-isotopologue.

Although the Brown et al. synthesis of trideuterated dihydroartemisinic acid is shorter than our 2021 study, the deuterated methyl Grignard reagent results in double bond regioisomers that are difficult to separate via basic flash column chromatography separations (HPLC purification is used).[4,5] With our 25-step synthesis, we avoided isomeric mixtures all together by employing a Grubbs ring closing metathesis to form the C4-C5 bond of DHAA,[7] and produced several compounds that could be used to test dihydroartemisinic acid analog bioactivity. Using $LiAlD_4$, we were also able to add deuteriums with >99% deuterium incorporation at C15 as determined by LCMS analysis.

4. SI Part 4: The Ene Reaction with Singlet Oxygen

A Shenck *ene* reaction involves an allylic C-H bond activated by the π-bond of molecular oxygen, replacing the C-H bond with a C- O bond (Figure S4-1). The mechanism of the Schenck *ene* reaction with $^1O_2$ has had discrepancies about whether it is a concerted or stepwise reaction due to the number of intermediates proposed.[65] The formation of a perepoxide between $^1O_2$ and simple alkenes has been supported by both computational and experimental work. Trisubstituted olefins have been shown prefer hydrogen abstraction on the more sterically hindered side of the double bond (names the *cis* effect). This suggests that the *ene* reaction doesn't occur through a simple six-membered concerted transition state.[66] Kinetic Isotope effects have been previously imployed to better understand the mechanism of the *ene* reaction. Previous studies on tetramethylethylene-d_6)[67] reported an intermolecular k_H/k_D = 1.04-1.41 which was proposed to support a perepoxide intermediate. Intermolecular ^{13}C isotope effects on d_{12}-2,3-dimethyl-2-butene ranging from 1.005-1.007, suggesting a simultaneous attack of $^1O_2$ to the double bond and bond formation to the olefinic carbons. Computational studies deduced that the reaction proceeds as a two-step no-intermediate mechanisms where the first transition state has perepoxide symmetry (with the hydrogen removal by singlet oxygen excluded), and then the second transition state nears a valley-ridge inflection (VRI) point, then after the VRI, the hydrogen from an alkyl group is removed.[65]

4. SI Part 4: The Ene Reaction with Singlet Oxygen

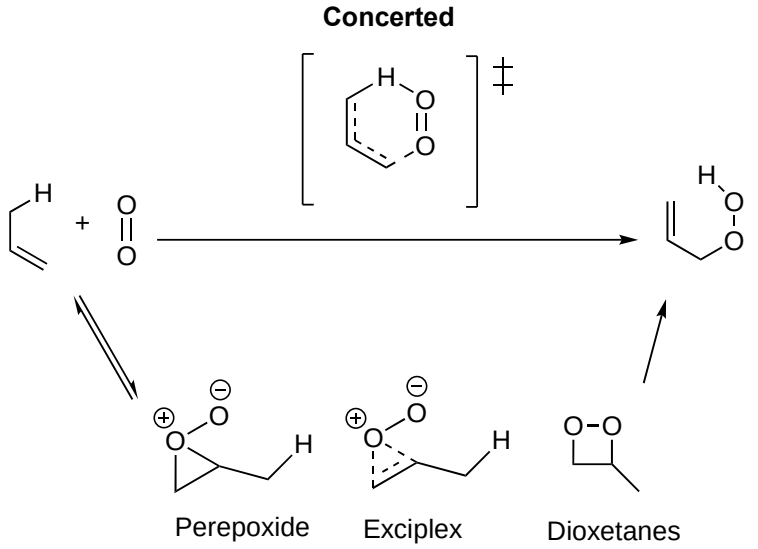

Figure S4-1. Various mechanisms proposed for the ene reaction with singlet oxygen.

Molecular oxygen exists in the atmosphere in its ground state as diatomic triplet oxygen ($^3\Sigma_g$) with the two electrons in its highest occupied molecular orbital (HOMO)[68] as two unpaired electrons with the same spin (Figure S4-2). When molecular oxygen is exposed to a photosensitizer and irradiated with light, the electrons in the HOMO become excited and one electron in the degenerate orbital flips and pairs with the electron in the other orbital to create oxygens first excited state ($^1\Delta_g$). One of the electrons can also flip to the opposite spin in its orbital, remaining unpaired, creating a higher energy second excited state ($^1\Sigma_g$). The first excited state is ~95 kJ/mol (~23 kcal/mol) higher in energy than ground state molecular oxygen, and the second excited state is very short lived with ~63 kJ/mol (~15 kcal/mol) higher energy then the first excited state.[69]

4. SI Part 4: The Ene Reaction with Singlet Oxygen

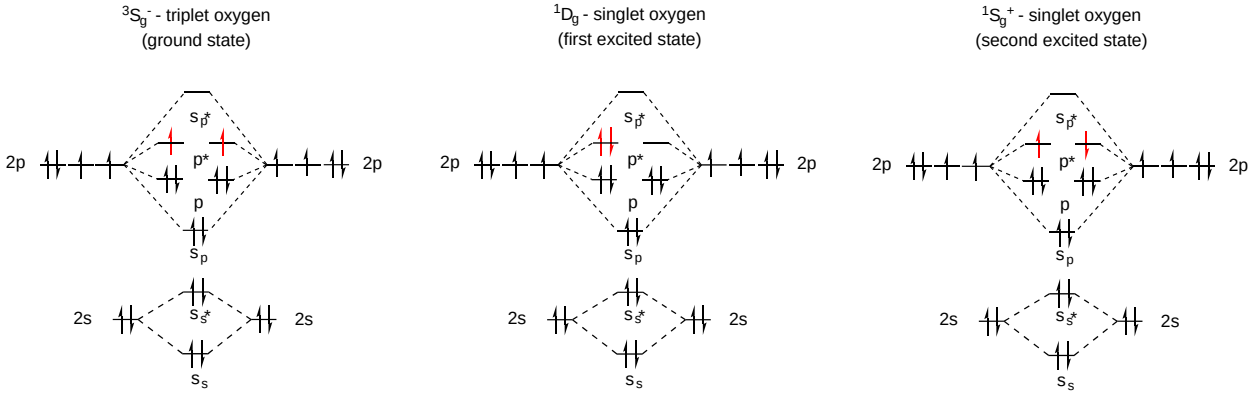

Figure S4-2. Electronic energy orbital diagram of triplet and singlet oxygen.

An arrow pushing mechanism is shown how singlet oxygen can form the perepoxide intermediate with DHAA (Figure S4-3). Figure S4-4A (left) and Figure S4-4B (right) show the two frontier molecular orbital interactions between:

(i) the HOMO of the π bonding molecular orbital of DHAA with the LUMO of the π* antibonding molecular orbital of $^1O_2$ (Figure S4-4A) and

(ii) the LUMO of the π* antibonding molecular orbital of DHAA with the HOMO of the π bonding molecular orbital of $^1O_2$ (Figure S4-4B)

4. SI Part 4: The Ene Reaction with Singlet Oxygen

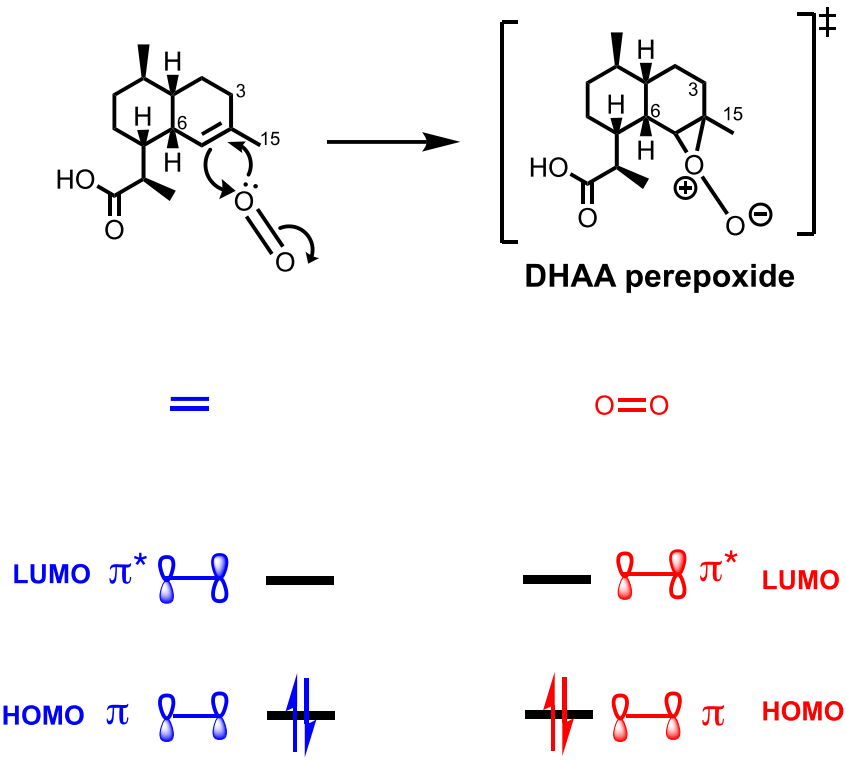

Figure S4-3. Singlet oxygen reacts with the alkene substrate through a perepoxide intermediate. A possible frontier molecular orbital interaction between the HOMO of the alkene and the LUMO of singlet oxygen is shown.

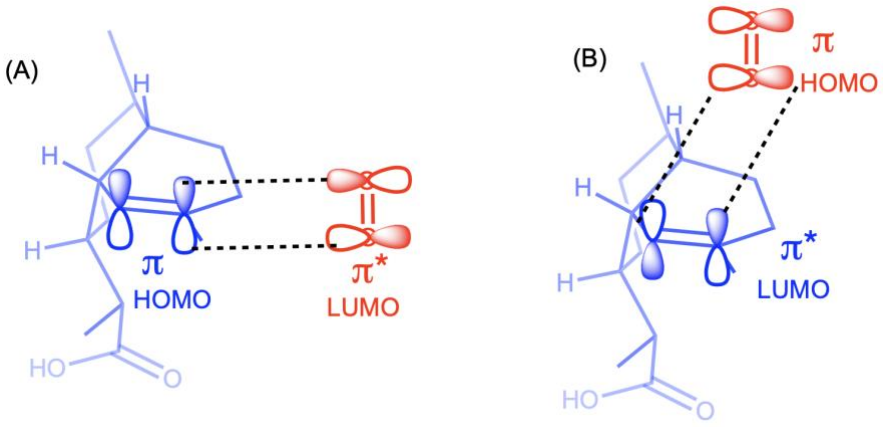

Figure S4-4. Possible frontier molecular orbital interactions between DHAA and singlet oxygen ($^1O_2$). (A) HOMO of DHAA and LUMO of $^1O_2$. (B) LUMO of DHAA and HOMO of $^1O_2$.

4. SI Part 4: The Ene Reaction with Singlet Oxygen

To determine the differences in reactivity of singlet oxygen with the DHAA isotopologues (**1**, **1b**, and **1c**), the compounds were treated with methylene blue in $CDCl_3$ in the presence of an LED flood lamp. Figure S4-5 shows the reaction and Figure S4-6 shows the NMR spectroscopic overlay between the different reactions. The bottom three rows are time point 0 minutes, and the top three rows are after shining the solution with light for 30 minutes.

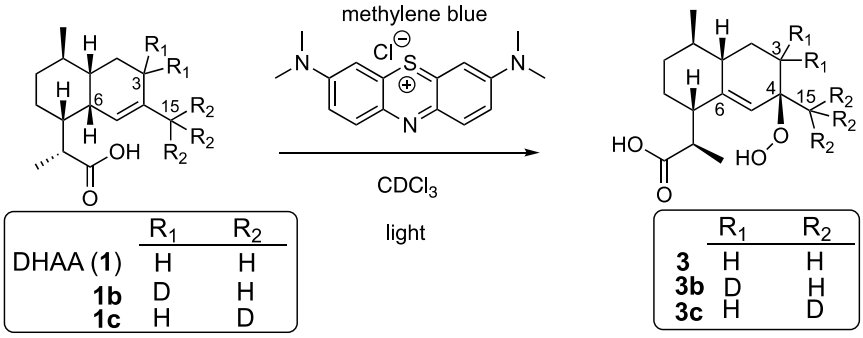

Figure S4-5. Reaction of singlet oxygen with DHAA isotopologues (**1**, **1b**, and **1c**).

Figure S4-6

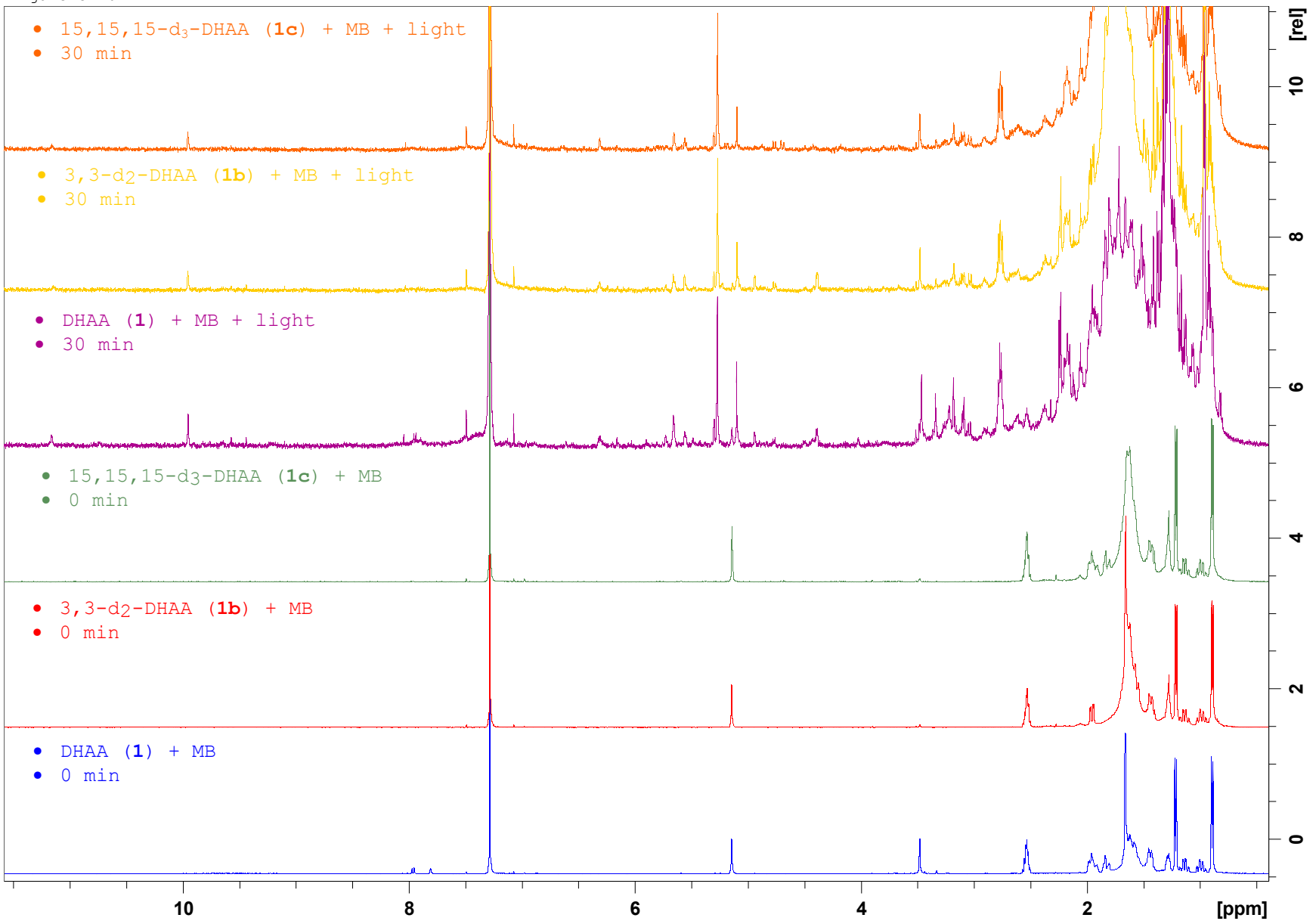

Figure S4-6. Singlet oxygen reaction with DHAA and methylene blue in $CDCl_3$. (also see main text Figure 23). Rows (i), (ii), (iii), (iv), (v), and (vi) (bottom to top): DHAA (1) and methylene blue (MB) at 0 minutes, 3,3-d_2-DHAA (1b) and methylene blue (MB) at 0 minutes, 15,15,15-d_3-DHAA (1c) and methylene blue (MB) at 0 minutes, DHAA (1) and methylene blue (MB) with light for 30 minutes, 3,3-d_2-DHAA (1b) and methylene blue (MB) with light for 30 minutes, 15,15,15-d_3-DHAA (1c) and methylene blue (MB) with light for 30 minutes.

5. SI Part 5: Triplet Oxygen Reaction with Allylic C-H Bonds

Reactions with triplet oxygen:

A trisubstituted silylallene was discovered to react with triplet oxygen to form a peroxide (Figure S5-1). This ene reaction involving an allenic C(sp^2)-H bond generating an alkyne with a propargylic peroxide had not been previously described in literature. When the subtracted was exposed to oxygen in the dark or under a sunlamp with a radical scavenger, the product was not observed, suggesting that the diradical form of triplet oxygen is involved.[70]

Because the reaction of triplet oxygen with singlet-state organic molecules is spin forbidden, organic substrates are oxidized with triplet oxygen using a radical autooxidation process.[71]

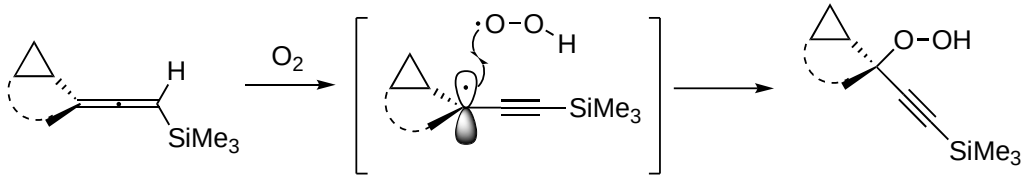

Figure S5-1. Triplet oxygen can react with a silyl allene compound.[71]

Linoleate autooxidation is thought to occur through either a radical isomerization or isomerization by reversible oxygen addition to yield hydroperoxide. 7-Dehydrocholesterol and isotachysterol (the acid catalyzed isomerization product of vitamin D_3 are also known to undergo autooxidation with radical mechanisms.[72,73]

6. SI Part 6: Alternative Reactions of DHAA with Oxygen

Acton and Roth found evidence for the incorporation of a mixture of unlabelled, mono- and di-labelled ^{18}O atoms into artemisinin based on the corresponding masses.[74] The IR spectrum experienced an upfield shift with the ^{18}O atoms incorporated in artemisinin. They also used $^{18}O_2$-induced chemical shifts in ^{13}C NMR spectroscopy. They reported upfield shifts of carbon **3** and **12a**, when two ^{18}O atoms were incorporated into the endoperoxide of artemisinin. They also showed that monolabelled ^{18}O was mostly at position **11** based of off comparison between the shifts of non-labelled and di-labelled artemisinin.

Another insight gained from the $^{18}O_2$ labeling experiment in was the fact that there were three different signals observed for the hemiacetal carbon (C12 in **2a**, **2b**, and **2c** in Figure S6-1) by ^{13}C NMR spectroscopy: δ 93.6173, 93.5898, and 93.5723. One interpretation of this result is that there are three different types of ^{18}O-incorporation mechanisms operating: (i) two mechanisms during endoperoxide formation where the hydroxy group of the carboxylic acid is dehydrated (i.e. Figure S6-1: mechanisms 1 and 2, to form **2a** and **2b**), and (ii) one with the original carboxylic acid oxygen from DHAA being retained in the lactone moiety of artemisinin (i.e. Figure S6-1: mechanism 3, to form **2c**).

Acton and Roth proposed several mechanistic pathways that explain the triplet oxygen oxidation of allylic hydroperoxide to artemisinin (Figure S6-1).[74] Air oxidation of the alkene on allylic hydroperoxide, followed by dioxetane formation can cleave open, then close to generate artemisinin. Allylic hydroperoxide could also go through an allylic rearrangement, then form dioxetane and cleave open to similar intermediate to the first mechanism described, and cyclized to artemisinin. In the second mechanism, the endoperoxide of artemisinin comes from the singlet oxygen oxidation of dihydroartemisinic acid, while in the first, the endoperoxide comes from

triplet oxygen. The third mechanism mentioned is where the peroxy group attacks the double bond of allylic hydroperoxide, resulting in a cyclic radical intermediate that autoxidized to peroxy hydroperoxide. The peroxy hydroperoxide could undergo ring expansion under acid catalysis and produce a carbocation that could close to artemisinin. If this mechanism occurs, the oxygen incorporated into the endoperoxide bridge of artemisinin would come from singlet oxygen.

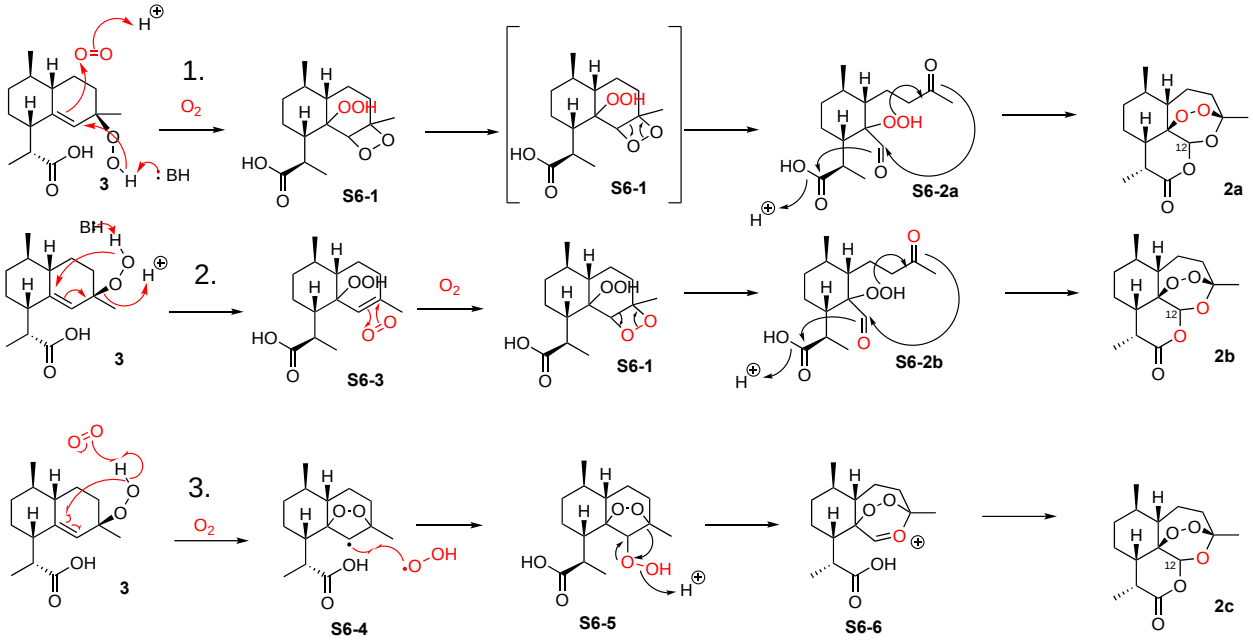

Figure S6-1. The 3 mechanisms proposed by Acton and Roth showing how DHAA-C4-hydroperoxide converts to artemisinin.[74]

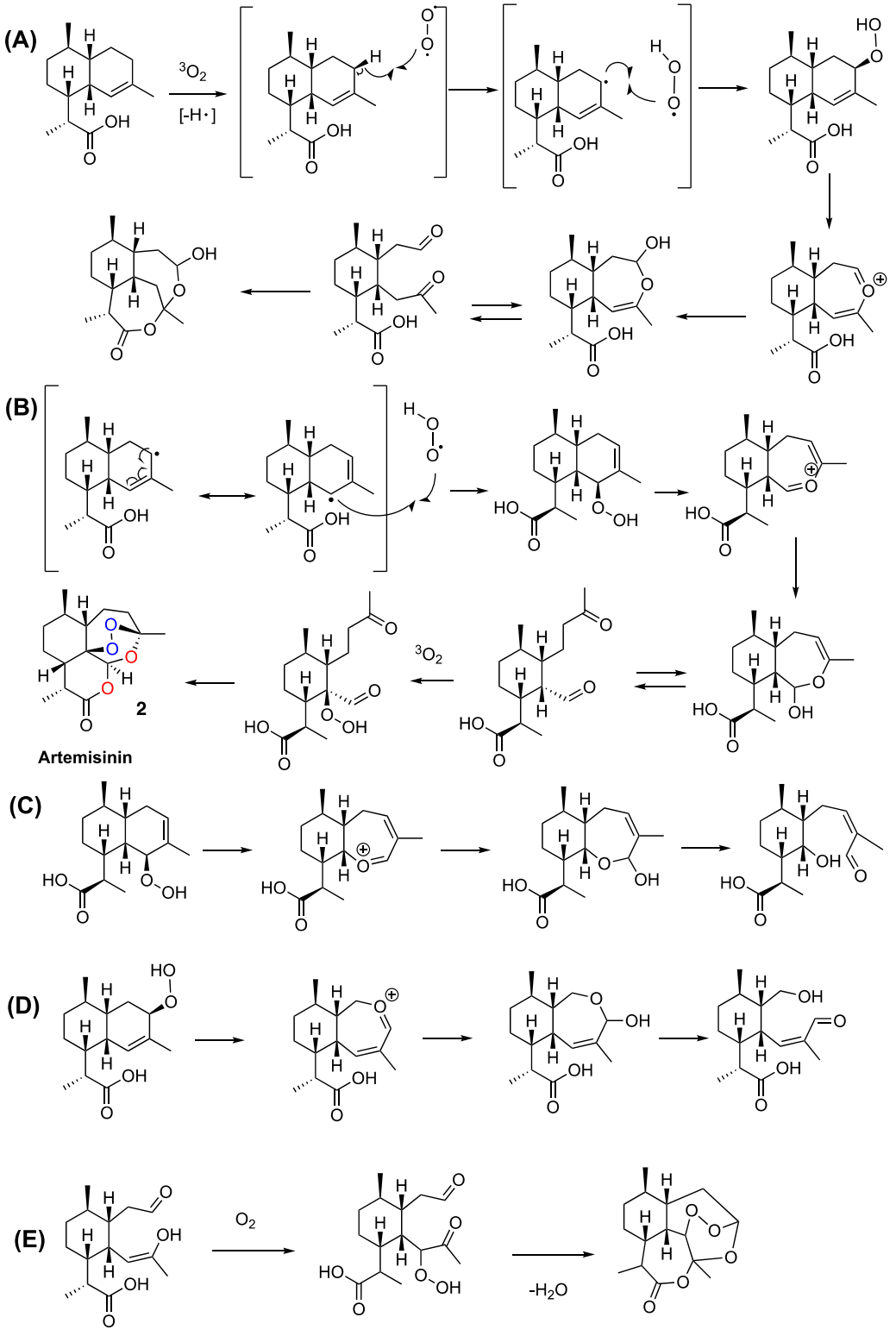

Figure S6-2. Oxidation of DHAA initiated by the abstraction of the C3-H bond by triplet oxygen to form (A) a C3-C4 bond cleaved product and (B) artemisinin.

6. SI Part 6: Alternative Reactions of DHAA with Oxygen

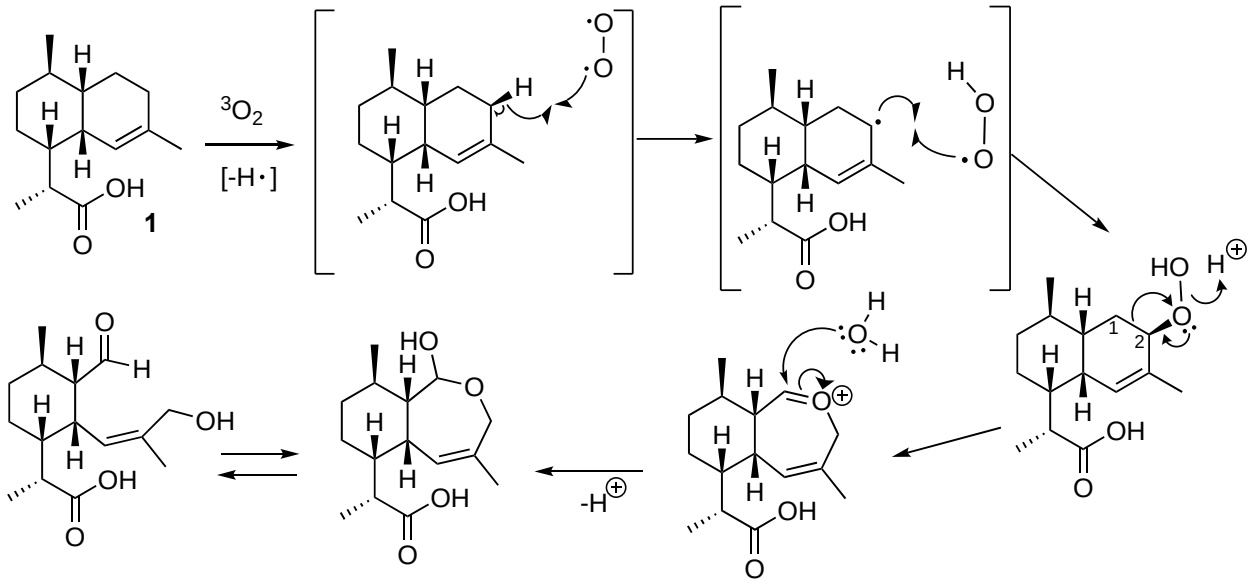

Figure S6-3. Hock cleavage could also potentially occur at C1-C2 on the allylic C2-hydroperoxide.

6. SI Part 6: Alternative Reactions of DHAA with Oxygen

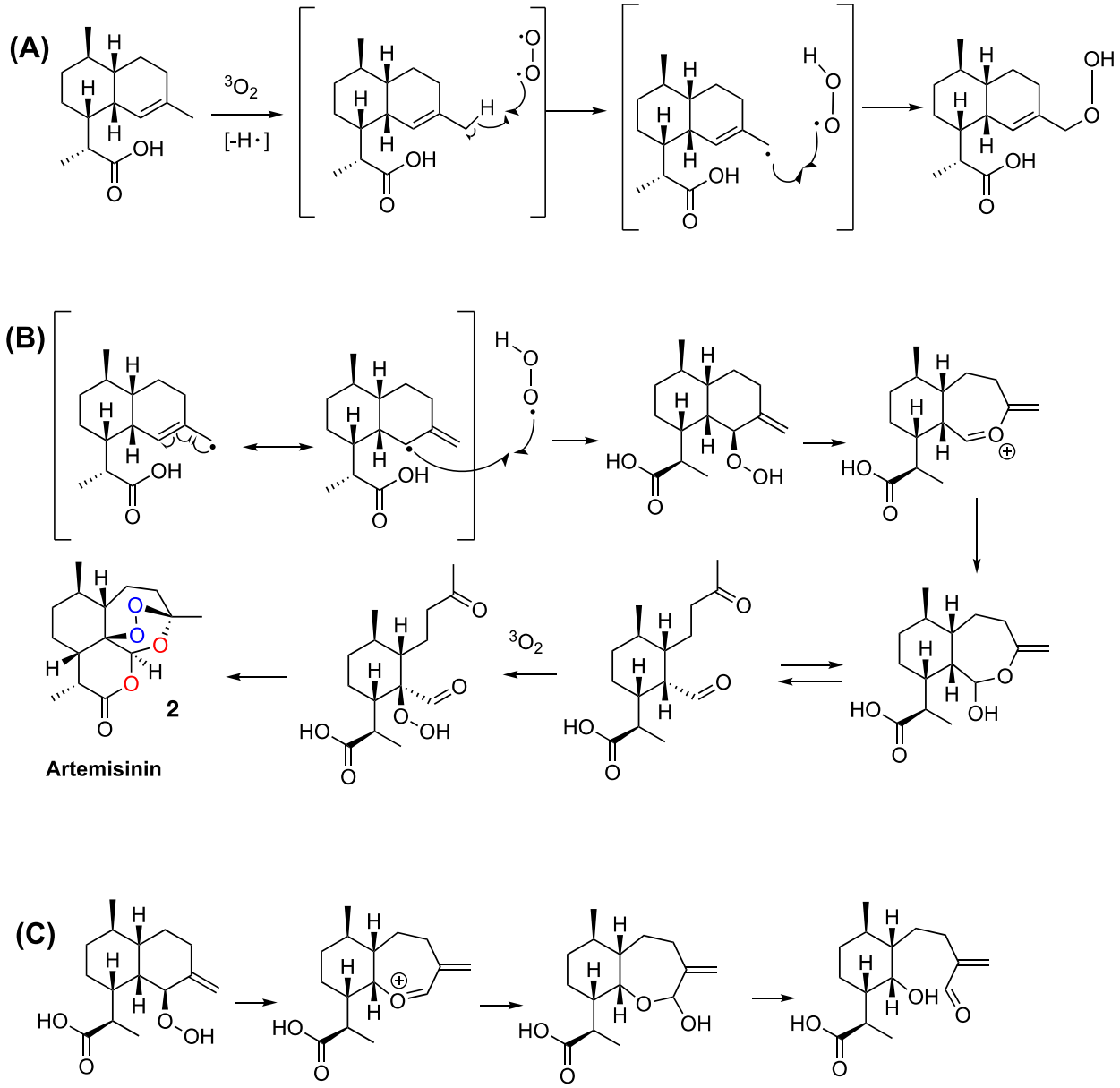

Figure S6-4. Oxidation of DHAA initiated by the abstraction of the C15-H bond by triplet oxygen to form (A) a C15-hydroperoxide and (B) artemisinin.

6. SI Part 6: Alternative Reactions of DHAA with Oxygen

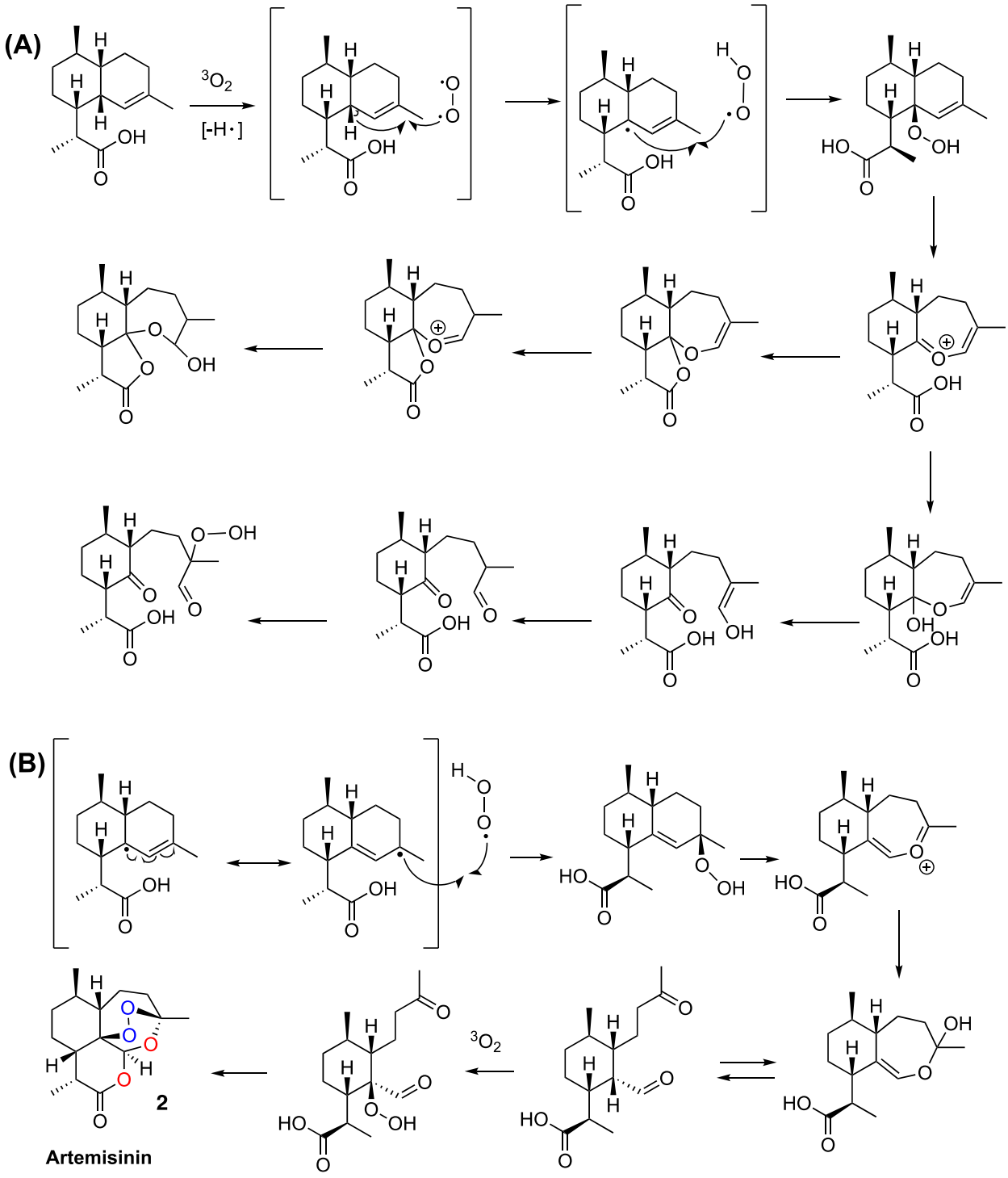

Figure S6-5. Oxidation of DHAA initiated by the abstraction of the C6-H bond by triplet oxygen to form (A) a C5-C6 bond cleaved product and (B) artemisinin.

7. SI Part 7: Bond Dissociation Energy Calculations of DHAA

Bond dissociation energies of DHAA were calculated using the following website:[75,76]

https://bde.ml.nrel.gov/result?name=CC1%3DCC2C%28CC1%29C%28C%29CCC2C%28C%29C%28%3DO%29O

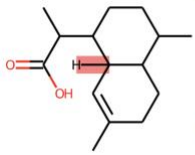

Bond 2

Bond Type: C-H

BDE(ML): *79.5 kcal/mol*

BDFE(ML): *70.1 kcal/mol*

Stereochemistry created

Neighbors

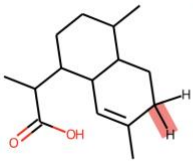

Bond 4

Bond Type: C-H

BDE(ML): *84.4 kcal/mol*

BDFE(ML): *75.1 kcal/mol*

Stereochemistry created

Neighbors

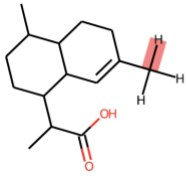

Bond 7

Bond Type: C-H

BDE(ML): *87.9 kcal/mol*

BDFE(ML): *79.7 kcal/mol*

Stereochemistry created

Neighbors

7. SI Part 7: Bond Dissociation Energy Calculations of DHAA

CC1CCC(C(C)C(=O)O)C2=CC(C)(OO)CCC21

Bond Dissociation Energies (from weakest to strongest)

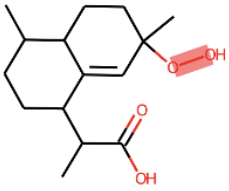

Bond 1

Bond Type: O-O
BDE(ML): *47.7 kcal/mol*
BDFE(ML): *36.4 kcal/mol*
Stereochemistry created
Neighbors

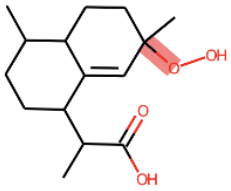

Bond 2

Bond Type: C-O
BDE(ML): *57.3 kcal/mol*
BDFE(ML): *43.6 kcal/mol*
Stereochemistry created
Neighbors

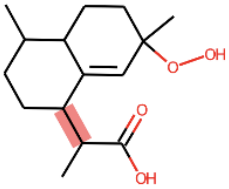

Bond 3

Bond Type: C-C
BDE(ML): *67.8 kcal/mol*
BDFE(ML): *52.8 kcal/mol*
Stereochemistry created
Neighbors

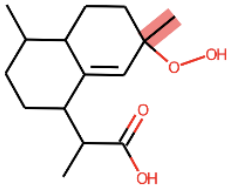

Bond 4

Bond Type: C-C
BDE(ML): *75.3 kcal/mol*
BDFE(ML): *61.0 kcal/mol*
Stereochemistry created
Neighbors

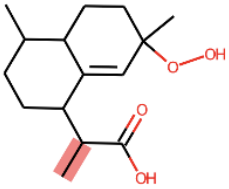

Bond 5

Bond Type: C-C
BDE(ML): *80.0 kcal/mol*
BDFE(ML): *65.8 kcal/mol*
Stereochemistry created
Neighbors

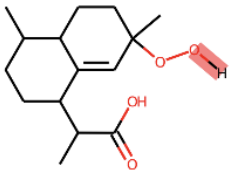

Bond 6

Bond Type: H-O
BDE(ML): *81.6 kcal/mol*
BDFE(ML): *73.5 kcal/mol*
Stereochemistry created
Neighbors

7. SI Part 7: Bond Dissociation Energy Calculations of DHAA

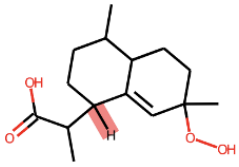

Bond 7

Bond Type: C-H
BDE(ML): *85.9 kcal/mol*
BDFE(ML): *76.7 kcal/mol*
Stereochemistry created
Neighbors

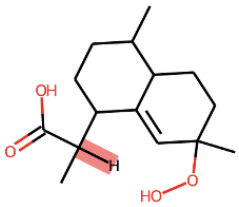

Bond 8

Bond Type: C-H
BDE(ML): *86.3 kcal/mol*
BDFE(ML): *77.3 kcal/mol*
Stereochemistry created
Neighbors

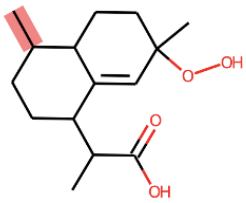

Bond 9

Bond Type: C-C
BDE(ML): *88.7 kcal/mol*
BDFE(ML): *74.7 kcal/mol*
Stereochemistry created
Neighbors

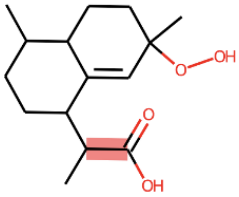

Bond 10

Bond Type: C-C
BDE(ML): *91.1 kcal/mol*
BDFE(ML): *76.4 kcal/mol*
Stereochemistry created
Neighbors

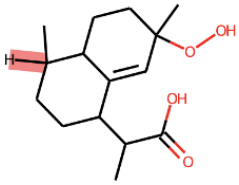

Bond 11

Bond Type: C-H
BDE(ML): *95.4 kcal/mol*
BDFE(ML): *86.0 kcal/mol*
Stereochemistry created
Neighbors

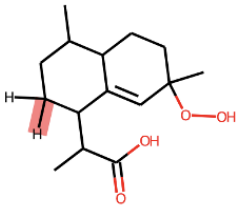

Bond 12

Bond Type: C-H
BDE(ML): *96.4 kcal/mol*
BDFE(ML): *87.3 kcal/mol*
Stereochemistry created
Neighbors

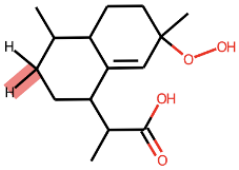

Bond 13

Bond Type: C-H
BDE(ML): *96.6 kcal/mol*
BDFE(ML): *87.5 kcal/mol*
Stereochemistry created
Neighbors

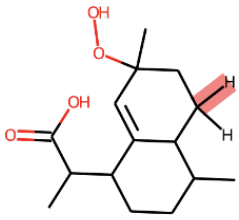

Bond 14

Bond Type: C-H
BDE(ML): *97.1 kcal/mol*
BDFE(ML): *88.0 kcal/mol*
Stereochemistry created
Neighbors

7. SI Part 7: Bond Dissociation Energy Calculations of DHAA

Bond 15

Bond Type: C-H
BDE(ML): *97.9 kcal/mol*
BDFE(ML): *89.1 kcal/mol*
Stereochemistry created
Neighbors

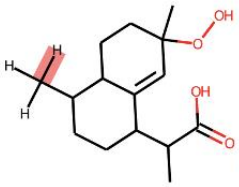

Bond 16

Bond Type: C-H
BDE(ML): *99.6 kcal/mol*
BDFE(ML): *90.6 kcal/mol*
Stereochemistry created
Neighbors

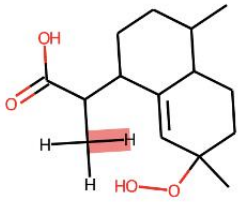

Bond 17

Bond Type: C-H
BDE(ML): *100.1 kcal/mol*
BDFE(ML): *91.0 kcal/mol*
Stereochemistry created
Neighbors

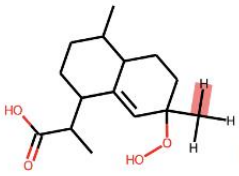

Bond 18

Bond Type: C-H
BDE(ML): *101.1 kcal/mol*
BDFE(ML): *92.2 kcal/mol*
Stereochemistry created
Neighbors

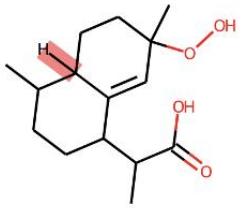

Bond 19

Bond Type: C-H
BDE(ML): *103.4 kcal/mol*
BDFE(ML): *94.7 kcal/mol*
Stereochemistry created
Neighbors

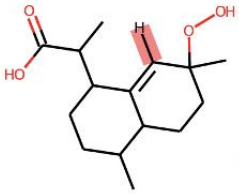

Bond 20

Bond Type: C-H
BDE(ML): *109.4 kcal/mol*
BDFE(ML): *100.8 kcal/mol*
Stereochemistry created
Neighbors

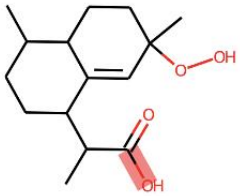

Bond 21

Bond Type: C-O
BDE(ML): *109.8 kcal/mol*
BDFE(ML): *98.0 kcal/mol*
Stereochemistry created
Neighbors

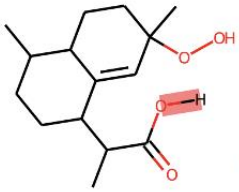

Bond 22

Bond Type: H-O
BDE(ML): *111.8 kcal/mol*
BDFE(ML): *102.9 kcal/mol*
Stereochemistry created
Neighbors

7. SI Part 7: Bond Dissociation Energy Calculations of DHAA

CC1=CC2C(CC1)C(C)CCC2C(C)C(=O)O

Bond Dissociation Energies (from weakest to strongest)

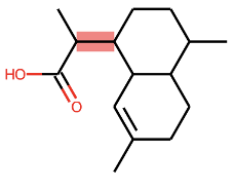

Bond 1

Bond Type: C-C
BDE(ML): *77.3 kcal/mol*
BDFE(ML): *61.8 kcal/mol*
Stereochemistry created
Neighbors

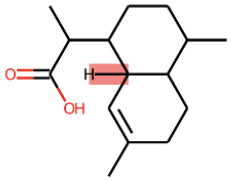

Bond 2

Bond Type: C-H
BDE(ML): *79.5 kcal/mol*
BDFE(ML): *70.1 kcal/mol*
Stereochemistry created
Neighbors

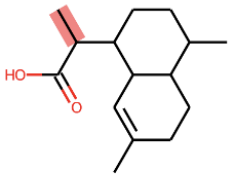

Bond 3

Bond Type: C-C
BDE(ML): *80.5 kcal/mol*
BDFE(ML): *66.3 kcal/mol*
Stereochemistry created
Neighbors

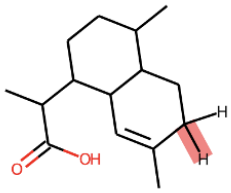

Bond 4

Bond Type: C-H
BDE(ML): *84.4 kcal/mol*
BDFE(ML): *75.1 kcal/mol*
Stereochemistry created
Neighbors

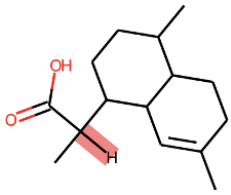

Bond 5

Bond Type: C-H
BDE(ML): *86.8 kcal/mol*
BDFE(ML): *77.7 kcal/mol*
Stereochemistry created
Neighbors

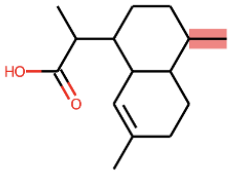

Bond 6

Bond Type: C-C
BDE(ML): *86.9 kcal/mol*
BDFE(ML): *72.7 kcal/mol*
Stereochemistry created
Neighbors

7. SI Part 7: Bond Dissociation Energy Calculations of DHAA

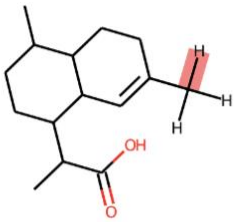

Bond 7

Bond Type: C-H
BDE(ML): *87.9 kcal/mol*
BDFE(ML): *79.7 kcal/mol*
Stereochemistry created
Neighbors

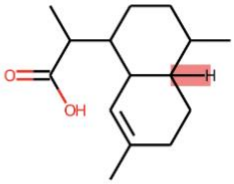

Bond 8

Bond Type: C-H
BDE(ML): *90.4 kcal/mol*
BDFE(ML): *81.3 kcal/mol*
Stereochemistry created
Neighbors

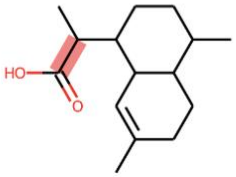

Bond 9

Bond Type: C-C
BDE(ML): *91.6 kcal/mol*
BDFE(ML): *76.9 kcal/mol*
Stereochemistry created
Neighbors

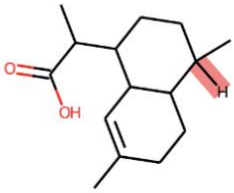

Bond 10

Bond Type: C-H
BDE(ML): *93.7 kcal/mol*
BDFE(ML): *84.2 kcal/mol*
Stereochemistry created
Neighbors

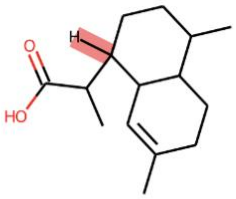

Bond 11

Bond Type: C-H
BDE(ML): *93.8 kcal/mol*
BDFE(ML): *84.2 kcal/mol*
Stereochemistry created
Neighbors

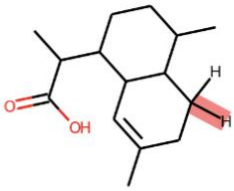

Bond 12

Bond Type: C-H
BDE(ML): *95.9 kcal/mol*
BDFE(ML): *86.9 kcal/mol*
Stereochemistry created
Neighbors

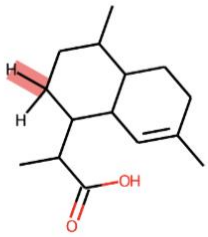

Bond 13

Bond Type: C-H
BDE(ML): *96.2 kcal/mol*
BDFE(ML): *87.1 kcal/mol*
Stereochemistry created
Neighbors

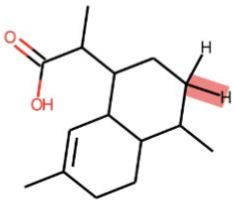

Bond 14

Bond Type: C-H
BDE(ML): *96.6 kcal/mol*
BDFE(ML): *87.5 kcal/mol*
Stereochemistry created
Neighbors

7. SI Part 7: Bond Dissociation Energy Calculations of DHAA

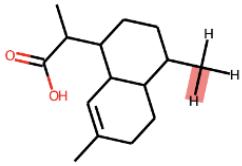

Bond 15

Bond Type: C-H
BDE(ML): *99.3 kcal/mol*
BDFE(ML): *90.3 kcal/mol*
Stereochemistry created
Neighbors

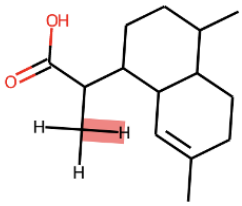

Bond 16

Bond Type: C-H
BDE(ML): *100.2 kcal/mol*
BDFE(ML): *91.1 kcal/mol*
Stereochemistry created
Neighbors

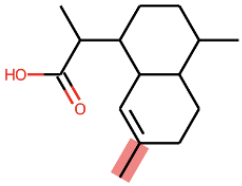

Bond 17

Bond Type: C-C
BDE(ML): *101.6 kcal/mol*
BDFE(ML): *88.5 kcal/mol*
Stereochemistry created
Neighbors

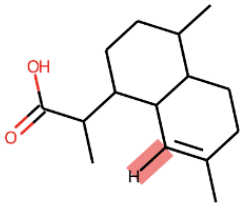

Bond 18

Bond Type: C-H
BDE(ML): *108.2 kcal/mol*
BDFE(ML): *99.7 kcal/mol*
Stereochemistry created
Neighbors

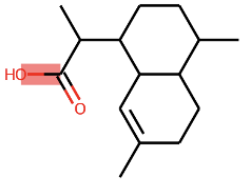

Bond 19

Bond Type: C-O
BDE(ML): *110.1 kcal/mol*
BDFE(ML): *98.3 kcal/mol*
Stereochemistry created
Neighbors

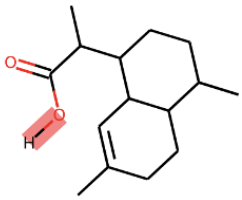

Bond 20

Bond Type: H-O
BDE(ML): *111.6 kcal/mol*
BDFE(ML): *102.7 kcal/mol*
Stereochemistry created
Neighbors

8. SI Part 8: LCMS Data to Detect DHAA Hydroperoxide (Main Text, Figure 22B)

(A)

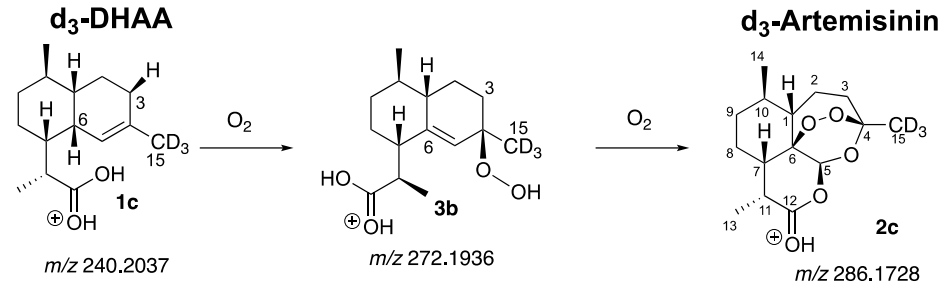

(B) 2 hr (C) 24 hr (D) 47 hr

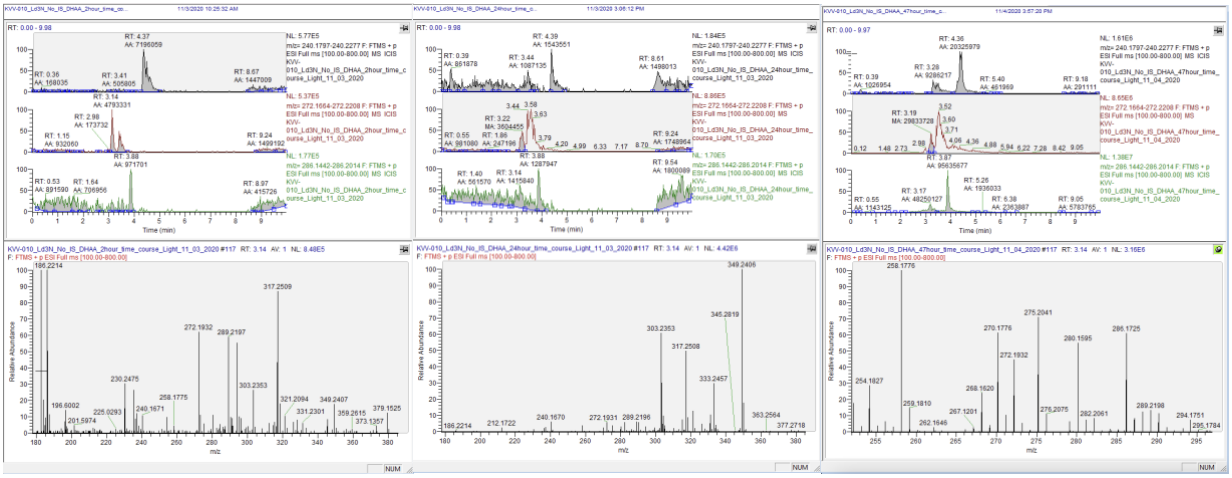

(E) 120 hr (F) 312 hr

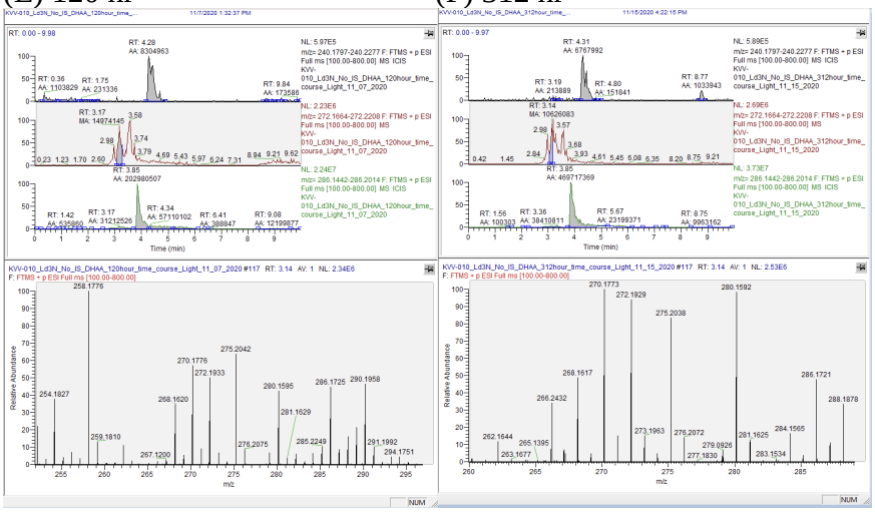

Figure S8-1. (A) A time course in monitoring spontaneous oxidation of d_3-DHAA (**1c**) to d_3-artemisinin (**2c**) through the hydroperoxide intermediate (**3b**) (data for Figure 22B of the main text). The time points taken were: (B) 2 hr, (C) 24 hr, (D) 47 hr, (E) 120 hr, and (F) 312 hr. Selected ion chromatograms are shown (top: *m/z* 240, middle: *m/z* 272, and bottom: *m/z* 286) and the mass spectrum corresponding to the retention time at 3.14 min, corresponding to the hydroperoxide ion (*m/z* 272) is shown for each time point.

9. SI Part 9: References for SI File

(1) Xing-Xiang, X.; Jie, Z.; Da-Zhong, H.; Wei-Shan, Z. Total synthesis of arteannuin and deozxyarteannuin. *Tetrahedron* **1986,** *42*, 819.

(2) Constantino, M. G.; Beltrame, M.; da Silva, G. V. J.; Zukerman-Schpector, J. A Novel Asymmetric Total Synthesis of (+)-Artemisinin. *Synthetic Communications* **1996,** *26*, 321.

(3) Rej, R. K.; Acharyya, R. L.; Nanda, S. Asymmetric synthesis of dihydroartemisinic acid through intramolecular Stetter reaction. *Tetrahedron* **2016,** *72*, 4931.

(4) Sy, L.-K.; Zhu, N.-Y.; Brown, G. D. Syntheses of dihydroartemisinic acid and dihydro-epi-deoxyarteannuin B incorporating a stable isotope label at the 15-position for studies into the biosynthesis of artemisinin. *Tetrahedron* **2001,** *57*, 8495.

(5) Brown, G. D.; Sy, L.-K. Synthesis of labelled dihydroartemisinic acid. *Tetrahedron* **2004,** *60*, 1125.

(6) Varela, K.; Arman, H. D.; Yoshimoto, F. K. Synthesis of [3,3-$^{2}H_{2}$]-Dihydroartemisinic Acid to Measure the Rate of Nonenzymatic Conversion of Dihydroartemisinic Acid to Artemisinin. *J. Nat. Prod.* **2020,** *83*, 66.

(7) Varela, K.; Arman, H. D.; Yoshimoto, F. K. Synthesis of [15,15,15-$^{2}H_{3}$]-Dihydroartemisinic Acid and Isotope Studies Support a Mixed Mechanism in the Endoperoxide Formation to Artemisinin. *J. Nat. Prod.* **2021,** *84*, 1967.

(8) Westfall, P. J.; Pitera, D. J.; Lenihan, J. R.; Eng, D.; Woolard, F. X.; Regentin, R.; Horning, T.; Tsuruta, H.; Melis, D. J.; Owens, A.et al. Production of amorphadiene in yeast, and its conversion to dihydroartemisinic acid, precursor to the antimalarial agent artemisinin. *PNAS* **2012,** *109*, E111.

(9) Bhonsle, J. B.; Pandey, B.; Deshpande, V. H.; Ravindranathan, T. New synthetic strategies towards (+)-artemisinin. *Tetrahedron Letters* **1994,** *35*, 5489.

(10) Yadav, J. S.; B.Thirupathaiah; Srihari, P. A concise stereoselective total synthesis of (+)-artemisinin. *Tetrahedron* **2010,** *66*, 2005.

(11) Wang, Z.; Yang, L.; Yang, X.; Zhang, X. Advances in the Chemical Synthesis of Artemisinin. *Synthetic Communications* **2014,** *44*, 1987.

(12) Dietrich, J. A.; Yoshikuni, Y.; Fisher, K. J.; Woolard, F. X.; Ockey, D.; McPhee, D. J.; Renninger, N. S.; Chang, M. C. Y.; Baker, D.; Keasling, J. D. A Novel Semi-biosynthetic Route for Artemisinin Production Using Engineered Substrate-Promiscuous P450BM3. *ACS Chemical Biology* **2009,** *4*, 261.

(13) Nabi, N.; Singh, S.; Saffeullah, P. An updated review on distribution, biosynthesis and pharmacological effects of artemisinin: A wonder drug. *Phytochemistry* **2023,** *214*, 113798.

(14) Hussain, A. Recent Trends on Production Sources, Biosynthesis Pathways and Antiviral Efficacies of Artemisinin: A Candidate Phytomedicine against SARS-CoV-2. *Curr. Pharm. Biotechnol.* **2023,** *24*, 1859.

(15) Zhao, L.; Zhu, Y.; Jia, H.; Zheng, X.; Wang, M.; Feng, W. Recent Trends on Production Sources, Biosynthesis Pathways and Antiviral Efficacies of Artemisinin: A Candidate Phytomedicine against SARS-CoV-2. *Molecules* **2022,** *27*, 6888.

(16) Huang, W.; Wang, Y.; Tian, W.; Cui, X.; Tu, P.; Li, J.; Shi, S.; Liu, X. Recent Trends on Production Sources, Biosynthesis Pathways and Antiviral Efficacies of Artemisinin: A Candidate Phytomedicine against SARS-CoV-2. *Antibiotics* **2022,** *11*, 1380.

(17) Tan, H. X.; Xiao, L.; Zhou, Z.; Zhang, L.; Chen, W. S. Molecular mechanism of artemisinin biosynthesis and regulation in Artemisia annua. *Zhongguo Zhong Yao Za Zhi* **2017,** *42*, 10.
(18) Srivastava, N.; Akhila, A. Biosynthesis of artemisinin- revisited. *Journal of Plant Interactions* **2011,** *6*, 265.
(19) Miziorko, H. M. ENZYMES OF THE MEVALONATE PATHWAY OF ISOPRENOID BIOSYNTHESIS. *Archives of Biochemistry and Biophysics* **2012,** *505*, 131.
(20) Thulasiram, H. V.; Poulter, C. D. Farnesyl Diphosphate Synthase: The Art of Compromise between Substrate Selectivity and Stereoselectivity. *J. Am. Chem. Soc.* **2006,** *128*, 15819.
(21) Firsov, A.; Mitiouchkina, T.; Shaloiko, L.; Pushin, A.; Vainstein, A.; Dolgov, S. Agrobacterium-Mediated Transformation of Chrysanthemum with Artemisinin Biosynthesis Pathway Genes. *Plants* **2020,** *9*, 537.
(22) Li, C.; Li, J.; Wang, G.; Li, X. Heterologous biosynthesis of artemisinic acid in *Saccharomyces cerevisiae*. *Journal of Applied Microbiology* **2016,** *120*, 1466.
(23) Marsafari, M.; Xu, P. Debottlenecking mevalonate pathway for antimalarial drug precursor amorphadiene biosynthesis in *Yarrowia lipolytica*. *Metab. Eng. Commun.* **2020,** *10*, e00121.
(24) Paddon, C. J.; Keasling, J. D. Semi-synthetic artemisinin: a model for the use of synthetic biology in pharmaceutical development *Nat. Rev. Microbiol.* **2014,** *12*, 355.
(25) Petzold, C. J.; Keasling, J. D. *Metabolic Engineering of Escherichia coli for the Production of a Precursor to Artemisinin, an Antimalarial Drug*; Wiley, 2011.
(26) Zeng, B.-X.; Yao, M.-D.; Wang, Y.; Xiao, W.-H.; Yuan, Y.-J. Metabolic Engineering of Saccharomyces cerevisiae for Enhanced Dihydroartemisinic Acid Production. *Front. Bioeng. Biotechnol.* **2020,** *8*, 152.
(27) Cobb, R. E.; Luo, Y.; Freestone, T.; Zhao, H. *Chapter 10 - Drug Discovery and Development via Synthetic Biology*, 2013.
(28) Meng, H.; Wang, Y.; Hua, Q.; Zhang, S.; Wang, X. *In silico* Analysis and Experimental Improvement of Taxadiene Heterologous Biosynthesis in *Escherichia coli*. *Biotechnology and Bioprocess Engineering* **2011,** *16*, 205.
(29) Ro, D.-K.; Paradise, E. M.; Ouellet, M.; Fisher, K. J.; Newman, K. L.; Ndungu, J. M.; Ho, K. A.; Eachus, R. A.; Ham, T. S.; Kirby, J.et al. Production of the antimalarial drug precursor artemisinic acid in engineered yeast. *Nature* **2006,** *440*, 940.
(30) Teoh, K. H.; Polichuk, D. R.; Reed, D. W.; Nowak, G.; Covello, P. S. *Artemisia annua* L. (Asteraceae) trichome-specific cDNAs reveal CYP71AV1, a cytochrome P450 with a key role in the biosynthesis of the antimalarial sesquiterpene lactone artemisinin. *FEBS Letters* **2006,** *580*, 1411.
(31) Brown, G. D.; Sy, L.-K. In vivo transformations of artemisinic acid in *Artemisia annua* plants. *Tetrahedron* **2007,** *63*, 9548.
(32) Zhang, Y.; Teoh, K. H.; Reed, D. W.; Maes, L.; Goossens, A.; Olson, D. J. H.; Ross, A. R. S.; Covello, P. S. The Molecular Cloning of Artemisinic Aldehyde ?11(13) Reductase and Its Role in Glandular Trichome-dependent Biosynthesis of Artemisinin in A*rtemisia annu*. *J. Biol. Chem.* **2008,** *283*, 21501.
(33) Polichuk, D. R.; Zhang, Y.; Reed, D. W.; Schmidt, J. F.; Covello, P. S. A glandular trichome-specific monoterpene alcohol dehydrogenase from *Artemisia annua*. *Phytochemistry* **2010,** *71*, 1264.

(34) Chang, M. C. Y.; Eachus, R. A.; Trieu, W.; Ro, D.-K.; Keasling, J. D. EngineeringEscherichia colifor production offunctionalized terpenoids using plant P450s. *Nature Chemical Biology* **2007,** *3*, 274.
(35) Huang, J. Q.; Fang, X. Amorpha-4,11-diene synthase: a key enzyme in artemisinin biosynthesis and engineering. *aBIOTECH* **2021,** *2*, 276.
(36) Abdallah, I. I.; van Merker, R.; Klumpenaar, E.; Quax, W. J. Catalysis of amorpha-4,11-diene synthase unraveled and improved by mutability landscape guided engineering. *Scientific Reports* **2018,** *8*, 9961.
(37) Picaud, S.; Mercke, P.; He, X.; Sterner, O.; Brodelius, M.; Cane, D. E.; Brodelius, P. E. Amorpha-4,11-diene synthase: Mechanism and stereochemistry of the enzymatic cyclization of farnesyl diphosphate. *Archives of Biochemistry and Biophysics* **2006,** *448*, 150.
(38) Pramastya, H.; Xue, D.; Abdallah, I. I.; Setroikromo, R.; Quax, W. J. High level production of amorphadiene using Bacillus subtilis as an optimized terpenoid cell factory. *New Biotechnology* **2021,** *60*, 159.
(39) Ro, D.-K.; Paradise, E. M.; Ouellet, M.; Fisher, K. J.; Newman, K. L.; Ndungu, J. M.; Ho, K. A.; Eachus, R. A.; Ham, T. S.; Kirby, J.et al. Prouction of the antimalarial drug precursor artemisinic acid in engineered yeast. *Nature* **2006,** *440*, 940.
(40) Feng, X.; Fan, S.; Lv, G.; Yan, M.; Wu, G.; Jin, Y.; Yang, Z. Expression, purification and X-ray crystal diffraction analysis of alcohol dehydrogenase 1 from *Artemisia annua* L. *Protein Expression and Purification* **2021,** *187*, 105493.
(41) Zhang, Y.; Teoh, K. H.; Reed, D. W.; Maes, L.; Goossens, A.; Olson, D. J. H.; Ross, A. R. S.; Covello, P. S. The Molecular Cloning of Artemisinic Aldehyde Δ11(13) Reductase and Its Role in Glandular Trichome-dependent Biosynthesis of Artemisinin in Artemisia annua. *J. Biol. Chem.* **2008,** *283*, 21501.
(42) Teoh, K. H.; Polichuk, D. R.; Reed, D. W.; Covello, P. S. Molecular cloning of an aldehyde dehydrogenase implicated in artemisinin biosynthesis in *Artemisia annua*. *Botany* **2009,** *87*, 635.
(43) Christianson, D. W. Structural and Chemical Biology of Terpenoid Cyclases. *Chemical Reviews* **2017,** *117*, 11570.
(44) Kim, S.-H.; Heo, K.; Chang, Y.-J.; Park, S.-H.; Rhee, S.-K.; Kim, S.-U. Cyclization Mechanism of Amorpha-4,11-diene Synthase, a Key Enzyme in Artemisinin Biosynthesis. *J. Nat. Prod.* **2006,** *69*, 758.
(45) Abdallah, I. I.; Czepnik, M.; van Merker, R.; Quax, W. J. Insights into the Three-Dimensional Structure of Amorpha-4,11-diene Synthase and Probing of Plasticity Residues. *J. Nat. Prod.* **2016,** *79*, 2455.
(46) Simtchouk, S.; Eng, J. L.; Meints, C. E.; Makins, C.; Wolthers, K. R. Kinetic analysis of cytochrome P450 reductase from Artemisia annua reveals accelerated rates of NADH-dependent flavin reduction *FEBS J.* **2013,** *280*, 6627.
(47) Yoshimoto, F. K.; Zhou, Y.; Peng, H. M.; Stidd, D.; Yoshimoto, J. A.; Sharma, K. K.; Matthew, S.; Auchus, R. J. Minor Activities and Transition State Properties of the Human Steroid Hydroxylases Cytochromes P450c17 and P450c21, from Reactions Observed with Deuterium-Labeled Substrates. *Biochemistry* **2012,** *51*, 7064.
(48) Geisler, K.; Hughes, R. K.; Sainsbury, F.; Lomonossof, G. P.; Rejzek, M.; Fairhurst, S.; Olsen, C. E.; Motawia, M. S.; Melton, R. E.; Hemmings, A. M.et al. Biochemical

analysis of a multifunctional cytochrome P450 (CYP51) enzyme required for synthesis of antimicrobial triterpenes in plants. *PNAS* **2013,** *110*, E3360.
(49) Bathe, U.; Tissier, A. Cytochrome P450 enzymes: A driving force of plant diterpene diversity. *Phytochemistry* **2019,** *161*, 149.
(50) Sohl, C. D.; Guengerich, F. P. Kinetic Analysis of the Three-step Steroid Aromatase Reaction of Human Cytochrome P450 19A1. *J. Biol. Chem.* **2010,** *285*, 17734.
(51) Yoshimoto, F. K.; Auchus, R. J. Rapid Kinetic Methods to Dissect Steroidogenic Cytochrome P450 Reaction Mechanisms. *J. Steroid Biochem. Mol. Biol.* **2016,** *161*, 13.
(52) Chowdhury, G. C.; Calcutt, M. W.; Guengerich, F. P. Oxidation of N-Nitrosoalkylamines by Human Cytochrome P450 2A6. *J. Biol. Chem.* **2010,** *285*, 8031.
(53) Bell-Parikh, L. C.; Guengerich, F. P. Kinetics of Cytochrome P450 2E1-Catalyzed Oxidation of Ethanolto Acetic Acid via Acetaldehyde. *J. Biol. Chem.* **1999,** *274*, 23833.
(54) Paddon, C. J.; Westfall, P. J.; Pitera, D. J.; Benjamin, K.; Fisher, K.; McPhee, D.; Leavell, M. D.; Tai, A.; Main, A.; Eng, D.et al. High-level semi-synthetic production of the potent antimalarial artemisinin. *Nature* **2013,** *496*, 528.
(55) Zhao, C.; Gao, Q.; Roberts, A. G.; Shaffer, S. A.; Doneanu, C. E.; Xue, S.; Goodlett, D. R.; Nelson, S. D.; Atkins, W. M. Cross-Linking Mass Spectrometry and Mutagenesis Confirm the Functional Importance of Surface Interactions between CYP3A4 and Holo/Apo Cytochrome b_5. *Biochemistry* **2012,** *51*, 9488.
(56) Kim, D.; Kim, V.; McCarty, K. D.; Guengerich, F. P. Tight binding of cytochrome b5 to cytochrome P450 17A1 is a critical feature of stimulation of C21 steroid lyase activity and androgen synthesis *J. Biol. Chem.* **2021,** *296*, 100571.
(57) Peng, H. M.; Liu, J.; Forsberg, S. E.; Tran, H. T.; Anderson, S. M.; Auchus, R. J. Catalytically Relevant Electrostatic Interactions of Cytochrome P450c17 (CYP17A1) and Cytochrome b_5. *J. Biol. Chem.* **2014,** *289*, 33838.
(58) Yoshimoto, F. K.; Guengerich, F. P. Mechanism of the Third Oxidative Step in the Conversion of Androgens to Estrogens by Cytochrome P450 19A1 Steroid Aromatase. *J. Am. Chem. Soc.* **2014,** *136*, 15016.
(59) McCarty, K. D.; Tateishi, Y.; Hargrove, T. Y.; Lepesheva, G. I.; Guengerich, F. P. Oxygen-18 Labeling Reveals a Mixed Fe−O Mechanism in the Last Step of Cytochrome P450 51 Sterol 14α-Demethylation. *Angewandte Chemie International Edition* **2024,** *63*, e202317711.
(60) Tateishi, Y.; McCarty, K. D.; Martin, M. V.; Guengerich, F. P. Oxygen-18 Labeling Defines a Ferric Peroxide (Compound 0) Mechanism in the Oxidative Deformylation of Aldehydes by Cytochrome P450 2B4. *ACS Catalysis* **2024,** *14*, 2388.
(61) Klayman, D. L. Qinghaosu (artemisinin): an antimalarial drug from China *Science* **1985,** *228*, 1049.
(62) Blasko, G., Cordell, G. A. . Definitive 1H- and 13C-NMR Assignments of Artemisinin (Qinghaosu). *J. Nat. Prod.* **1988,** *51* (6), 1273.
(63) Sy, L.-K.; Brown, G. D. The mechanism of the spontaneous autoxidation of dihydroartemisinic acid. *Tetrahedron* **2002,** *58*, 897.
(64) Want, E. J.; Cravatt, B. F.; Siuzdak, G. The expanding role of mass spectrometry in metabolite profiling and characterization *Chembiochem* **2005,** *6*, 1941.
(65) Orfanopoulos, M. Singlet Oxygen: Discovery, Chemistry, C60-Sensitization. *Photochem. Photobiol.* **2021,** *97*, 1182.

(66) Orfanopoulos, M., Grdina. S. M., Stephenson, L. M. . Site specificity in the singlet oxygen-trisubstituted olefin reaction. *J. Am. Chem. Soc.* **1979,** *101* (1), 275.
(67) Grdina, M. B., Orfanopoulos, M., Stephenson, L. M. . Stereochemical Dependence of Isotope Effects in the Singlet Oxygen-Olefin Reaction. *J. Am. Chem. Soc.* **1979,** *101* (11), 3111.
(68) Stuhr, R.; Bayer, P.; von Wangelin, A. J. The Diverse Modes of Oxygen Reactivity in Life & Chemistry. *ChemSusChem* **2022,** *15*, e202201323.
(69) Keszthelyi, T., Weldon, D., Anderson, T. N., Poulsen, T. D., Mikkelsen, K. V., Ogilby, P. R. . Radiative Transitions of Singlet Oxygen: New Tools, New Techniques and New Interpretations. *Photochem. Photobiol.* **1999,** *70* (4), 531.
(70) Xia, Y., Lee, N-K. Sabbasani, V. R., Gupta, S., Lee, D. . Reaction of silylallenes with triplet molecular oxygen. *Org. Chem. Front.* **2018,** *5*, 2542.
(71) Kananovich, D., Elek, G. Z., Lopp, M. Borovkov, V. . Aerobic Oxidations in Asymmetric Synthesis: Catalytic Strategies and Recent Developments. *Front. Chem.* **2021,** *9: 614944*.
(72) Jin, X., Yang, X., Yang, L., Liu, Z-L., Zhang, F. . Autoxidation of isotachysterol. *Tetrahedron* **2004,** *60*, 2881.
(73) Porter, N. A. A Perspective on Free Radical Autoxidation: The Physical Organic Chemistry of Polyunsaturated Fatty Acid and Sterol Peroxidation. *J. Org. Chem.* **2013,** *78* (8), 3511.
(74) Acton, N.; Roth, R. J. On the Conversion of Dihydroartemisinic Acid into Artemisinin. *J. Org. Chem.* **1992,** *57*, 3610.
(75) St. John, P. C.; Guan, Y.; Kim, Y.; Etz, B. D.; Kim, S.; Paton, R. S. Quantum chemical calculations for over 200,000 organic radical species and 40,000 associated closed-shell molecules. *Sci. Data* **2020,** *7*, 244.
(76) St. John, P. C.; Guan, Y.; Kim, Y.; Kim, S.; Paton, R. S. Prediction of organic homolytic bond dissociation enthalpies at near chemical accuracy with sub-second computational cost. . *Nat. Commun.* **2021,** *11*, 2328.